Hindawi
Advances in Civil Engineering
Volume 2023, Article ID 2756105, 23 pages
https://doi.org/10.1155/2023/2756105

Research Article

Numerical Studies of Floor Heave Control in Deep Mining Roadways with Soft Rocks by the Rock Bolts Reinforcement Technology

Ivan Sakhno and Svitlana Sakhno

Donetsk National Technical University, 29 Sofia Kovalevska Street, Lutsk, Volyn Region 43012, Ukraine

Correspondence should be addressed to Ivan Sakhno; ivan.sakhno@donntu.edu.ua

Received 19 October 2022; Revised 6 November 2022; Accepted 24 November 2022; Published 27 January 2023

Academic Editor: Pengjiao Jia

The floor heave is one of the key factors that can restrict high-efficiency and safety mining, especially in the deep roadways with soft rock. Considering the influences of rock fracturing over time on rock mass properties, a case study of the floor heave evolution and rock bolts reinforcement technology was performed in this paper. A numerical simulation was used to study the stress-strain state and displacement of surrounding rocks. It was found that significant floor heave caused by nonlinear deformation of laminated immediate floor under an increase in rock fracturing. The post-peak strain regions appear in the bottom corners of the roadway, after which strata in the immediate floor are destroyed one by one. The joint spacing of 0.45 m on the immediate floor is critical. At this step, post-peak strain regions merge in the central part of the roadway floor, which is the cause of uncontrolled floor heave. Rock bolts reinforcement was proposed to control the floor heave. Three floor support schemes with two types of support elements, different bolt orientations, and lengths of reinforcement were studied. The numerical simulation demonstrated that after reinforcement, post-peak plastic strain in the floor strata was reduced effectively. The optimal floor support scheme and depth of reinforcement were determined by the allowable floor heave. Ideally, the floor heaves could be reduced by rock bolts with a steel belt installed according to the support scheme III and reinforcement length of 2.0 m for outer bolts and 3.0 m for central bolts.

1. Introduction

With the increase in mining depth, the instability of roadways in soft rock has become a major challenge for deep coal mines [1, 2]. According to statistics, the actual repair rate of roadways in Ukraine is as high as 80%. A similar repairing rate is noted by researchers from other countries [3, 4]. The instability problems that are exacerbated due to deep mining are roadway surrounding rock large deformation, floor heave, support failure, and roof fall. In the case of the rock mass composed of soft fissured rock, the roadways stability issue is further relevant.

Current roadway support systems, including rock bolting, steel arch, hydraulic supports, and combined supports, are commonly successfully used to control the deformation of the roof and side walls of roadways. However, often a floor heave is still a serious failure phenomenon in mine roadways [5–7].

Many scholars have used theoretical analysis, physical experiments, and numerical simulations to study the floor heave in deep roadways with soft rock and have proposed various solutions. Existing technologies of floor heave controlling are quite advanced; these include the steel closed supports and concrete inverted arches, stress relief slots in the floor or wall of roadway, and reinforcement of surrounding rock.

Zhao et al. [8] researched and proposed a U-shaped steel closed support with an inverted steel arch in the floor as a method for improving the support effect of the surrounding rock during the process of floor heaving. Li et al. proposed the double-yield shell coupling support technology for high-stress soft rock roadways [9]. Wang et al. [10] managed to

control floor heave by using the high resistance yieldable multiple support for roadways excavated in extremely soft rocks.

Zheng et al. [11] designed a composite structure, including concrete antiarches and bolts, to control the floor heave. By means of field investigation, theoretical analysis, numerical calculation, and engineering practice. Wang et al. [12] established the instability reasons for the inverted arch structure and proposed a 36U-shaped steel round frame with bolt-mesh-shotcrete-combined support to control the floor heave.

Chen et al. [13] proposed an innovative "relief-retaining" control scheme of floor heave, which is the comprehensive measure of "cutting groove in floor + drilling for pressure relief at roadway side + setting retaining piles at the junction of roadway side and floor." Yang and Zhang [14] put forward the pressure-relief slot to prevent floor heave, established the mechanical model of the pressure-relief slot, and gave a method to determine the width of the pressure-relief slot.

The most worldwide floor heave control technology is reinforcement. Chang et al. [15] proposed hydraulic expansion bolts to prevent the development and flow of the plastic zone in the floor rock to control floor heave. He et al. [16] proposed a new method to control floor heave with bolt-net-anchor coupling support technology, with the anchor wire at a key location, with the rigid bolt, and corner grouting. Yang et al. [17] studied the floor heave control method of high-stress soft rock roadway and proposed new coupling support technology of a bolt-mesh-anchor-base angle bolt-flexible layer truss for controlling roadway floor heave. Wang et al. [18], using numerical simulations and theoretical analysis determined that an effective method for controlling floor heave is "self-drilling anchor bolt" + "high-strength reinforcement anchor bolt" + "W type steel belt" + "steel mesh" + anchor cable with birdcage.

Some scholars have focused on the bottom corners of the roadway where the critical stress concentration causes failure. Chen et al. [19] controlled the floor heave of gob-side entry retaining by reinforcing sides and corners of the solid coal body, and obtained an influence on the floor heave of gob-side entry retaining of sides supporting strength and the bottom bolt orientation in coal side. Cao et al. [20], based on the modelling by FLAC3D, proposed the floor support method, which includes optimal bolt parameters and arrangement, floor beam layout by grooving, and full-length grouting. Guo et al. [21] showed that intensive bolts with steel belt, wire mesh, and cable, can significantly reduce the floor heave in the roadway, the roof, and the side walls, compared with lower supporting intensity.

Zhang and Shimada [22] managed to control floor heave in retained goaf-side gate road by using grouting reinforcement. Shimada et al. [23] studied the reinforcement effect of cement grouting materials with different water-cement ratios on the floor. Sun et al. put forward the technology of reinforcing surrounding rocks to realize floor stability in inclined strata and soft rock [24].

To solve the problem of roadway floor heave, Zhou et al. [25] put forward three rock bolt support optimization schemes. The support effect of each scheme was simulated and finally was determined that scheme 3 (the base plate anchor bolt adopts a pair of bottom angle anchor bolts in each row plus three vertical anchor bolts) is the best support optimization scheme.

Most studies are based on the results of numerical simulations because there are the best ways to model the magnitudes and spatial distribution of deformations [26]. Zhao et al. [8], Chen et al. [13], Guo et al. [21], Zhang and Shimada [22], and Zhou et al. [27] used a FLAC3D simulation. Kulatilake et al. used 3DEC software to simulate high-stress roadways and proposed the use of 3 m bolts and inverted arch roadways to control the surrounding rock [25]. Qi et al. [3], and Zhang et al. [28] simulated the failure mechanism of soft rock roadway by UDEC. Sakhno et al. [29] performed numerical modelling of controlling a floor heave of roadways in the soft rock by ANSYS. Małkowski et al. [26] used a phase 2 program.

In this paper, the mine roadway floor heave evolution during an increase in rock fracturing over time and rock bolts reinforcement technology were studied to effectively control the large nonlinear deformation of soft laminated floor rock. The mechanical properties of the surrounding rocks were studied using laboratory tests. The floor heave evolution and characteristics of the stress-strain state of surrounding rocks were analyzed by using the ANSYS. At the same time, physical and mechanical properties of the rocks were changed during the simulation. The degree of rock mass discontinuity was carried out by changing the Hoek–Brown parameters. This paper proposed coupling floor support technology of rock bolts with steel belt, which includes optimal bolt parameters and arrangement. The specific parameters suitable for controlling the floor heave of the roadway were determined using the numerical simulation method.

2. Engineering Background

2.1. Project Overview. Surgaya coal mine is located in Vugledar city, Donbas region of Ukraine. At present, the main producing coal seam is the C11 coal seam. The average thickness of the C11 coal seam is 1.6 m, while the dip angle ranges from 7° to 10°. The studied roadway is presented in Figure 1(a). It was an air-return roadway of the 14th eastern panel of level 824 m. The dip angle of the roadway was 8°. The width and length of the 13th eastern panel were 182 m and 1600 m, respectively. This panel was extracted. At present, the 14th eastern transport roadway is being developed to create a new 14th eastern longwall panel. There are 45 m and 56 m coal pillars between the air-return roadway of the 14th eastern panel and the stop mining line. The surrounding rock of the roadway is mainly composed of mudstone and sandy mudstone. The detailed strata histogram and position of the roadway are illustrated in Figure 1(b).

2.2. Supporting System and Deformation Characteristics. The section shape of the studied roadway was a semi-circular arch, 5.5 m in width and 4.2 m in height. The height of the straight wall was 1.8 m and the radius of the arch was 2.64 m.

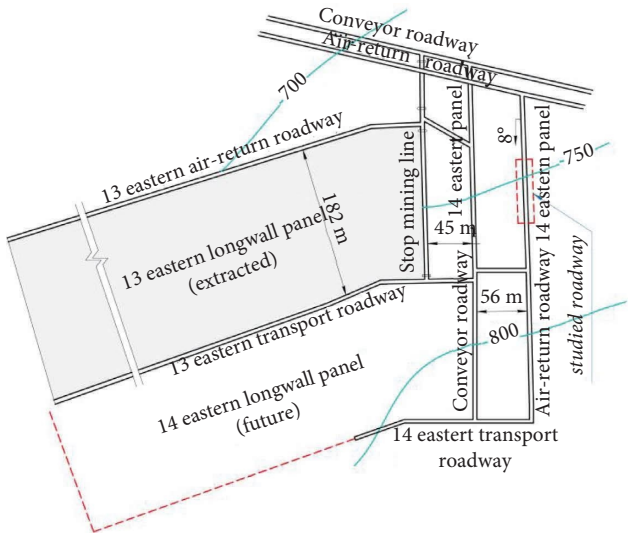

(a)

Column	Lithology	Thickness (m)	Geologic description, uniaxial strength σ_c, (MPa)
	sandy mudstone	21.2	gray, horizontal bedding, σ_c=30-35 MPa
	sandy mudstone	8.6	dark gray, σ_c=22 MPa
	coal C11	1.4	semibright coal, fractured, σ_c=7-10 MPa
	mudstone	6.0	gray, laminated σ_c=18.5 MPa
	sandstone	22.5	gray, horizontal bedding, σ_c=32-37 MPa

(b)

Figure 1: The studied area and geological conditions: (a) the locations of the studied roadway; (b) strata histogram.

The support used in the roadway was U-shape steel arches (U33) with wooden boards as filling material.

Field observations revealed a serious overall deformation of the roadway that has significantly reduced the roadway section. The characteristic points of failure of the roadway were the roof, floor, and roadway side walls.

The average roof subsidence and side walls convergences were 370 mm and 280 mm, respectively. In some sections of the roadway, the rate of deformation was as large as 1.5 times. This was the reason for the failure of the legs and the shed top of U-shaped steel arches (Figures 2(a) and 2(b)). As a rule, these locations were associated with different degrees of water inflow. Despite this, the deformations of the roof and side walls overall were not critical. The main problem was a floor heave up to 0.5-0.6 m (Figure 2(c)). The floor heave was aggravated in zones of the increased water content of the rocks. The deformation and failure of the roadways and supports are shown in Figure 2(d). The track laid in the roadway was seriously deformed. The roadway had to be repaired to ensure transport and supply the necessary amount of air to ventilate the 13 longwall panels. This process wasted a lot of manpower and material resources. So, it is necessary to optimize the support scheme to control the floor heave of the roadway and ensure the normal production of the 14th longwall panel and the next ones after it.

The results of observation are in good agreement with measurements in situ. The floor heave on stations, which were built in roadways D-2 and F-33b, was monitored over two years [30]. In roadway D-2, the maximum value of upheaval after almost 800 days of monitoring was 0.54 m, and in roadway F-33b 0.6 m. The average value of floor heave on monitoring stations in the conveyor roadway of 5 longwalls of 3 m seam was 0.7 m [31]. The zone of rock cracking in the floor of the roadway was more than 7 m. The floor heave of the roadway of the Qitaihe Longhu coal mine [27] was very serious; the maximum floor heave was 0.9 m, which seriously restricted the efficient production of the coal mine.

2.3. Laboratory Tests. The specimens of intact rocks were selected during excavated of the floor and reconstruction of the roadway for the uniaxial compressive strength tests. Rectangular prism-shaped specimens with a rib size of about 55 mm were made. The tests were completed using a universal testing machine (Figure 3(a)). Test results for a specimen of mudstone and coal are shown in (Figure 3(b)) as an example.

Then, the average deformation modulus (E_{def}) was calculated in the pre-peak region of the stress-strain curve. The deformation modulus fluctuations for the last stage of loading of specimens are shown in Figure 3(b). The average value of E_{def} of mudstone was 1955 MPa, and E_{def} of coal was 1145 MPa. The uniaxial compressive strength (σ_c) of mudstone was 19.3 MPa, and (σ_c) of coal was 9.1 MPa.

Due to the previous long exploitation time of the roadway (more than 4 years), and water inflow the surrounding soft rocks were fractured. Therefore, to model rock masses, it is necessary to correct the parameters of intact rock.

The Hoek–Brown Failure Criterion [32] was used, which is widely accepted and applied in many projects and applications around the world. Based on the physical and mechanical measurements and analysis of the joint, the surrounding rocks were determined Hoek–Brown Parameters: the Geological Strength Index (GSI), values of the constant m_i and the disturbance factor (D). For example, the Hoek–Brown parameters used the modelling for the floor rocks not exposed to the water and for the waterlogged floor rocks in the project [26].

Since the main problem with the stability of the roadway was floor heaving, floor rocks were studied more carefully.

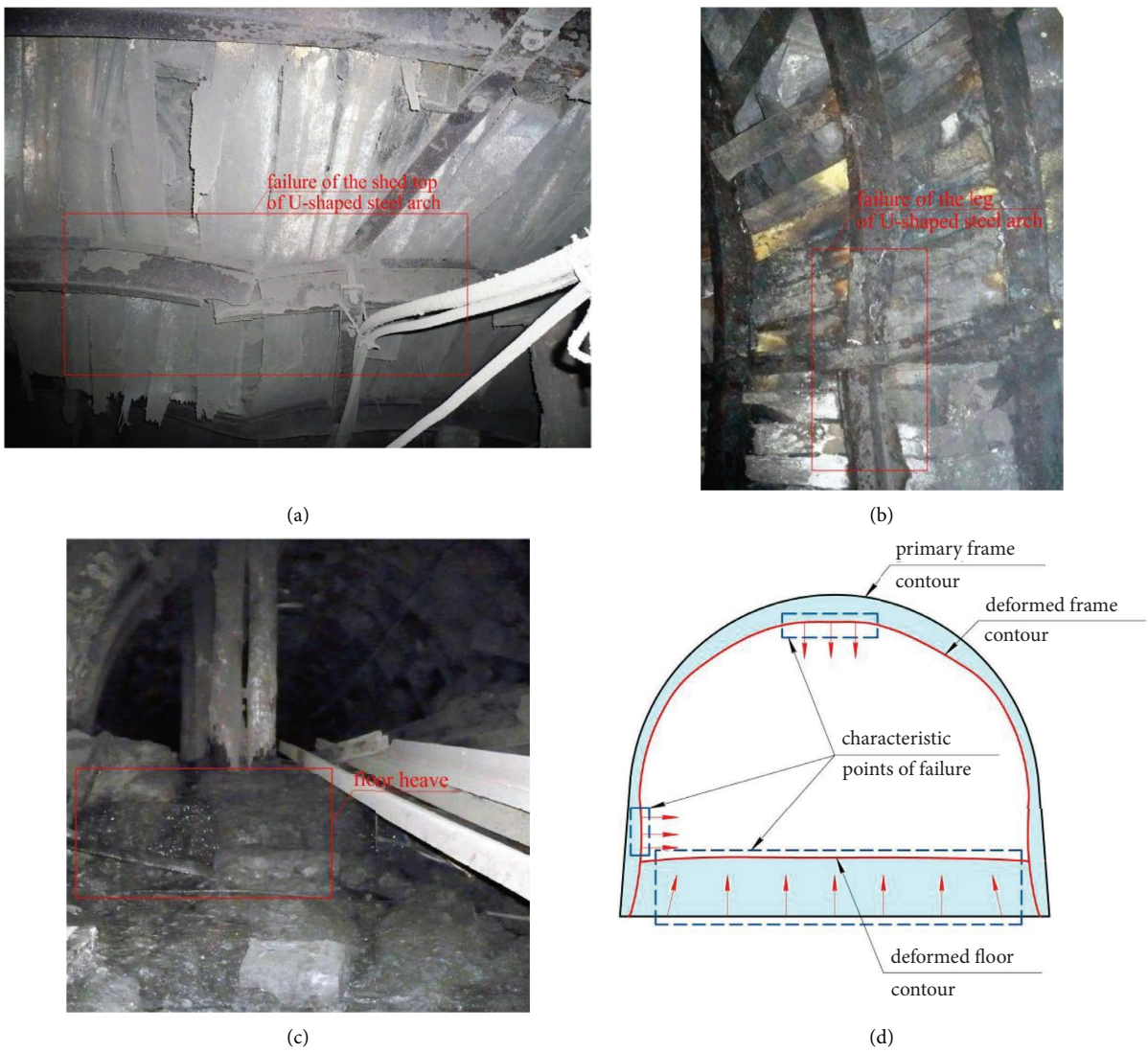

Figure 2: The characteristics of rupture of the roadway: (a) the failure of the shed top of the U-shaped steel arch; (b) the failure of the leg of the U-shaped steel arch; (c) the floor heave; (d) the characteristic failures of the studied roadway.

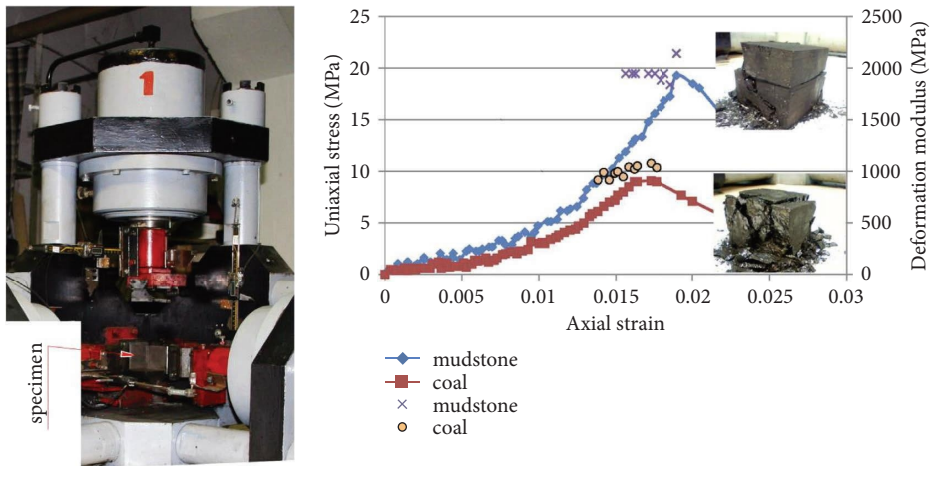

Figure 3: Laboratory equipment and test results: (a) the universal testing machine; (b) stress-strain curve and deformation modulus fluctuations for coal and mudstone specimens.

The study of the degree of disturbance of floor rock mass showed that the average joint spacing was about 30 cm, so the minimum GSI value was taken to be 63 (Figure 4) [33]. The disturbance factor for the floor was $D = 0.7$.

The Geological Strength Index for surrounding rocks was calculated as GSI = RMR_{89}−5 [26, 32], and it has been in the range of 74–63 since mining, as shown in Figure 4.

For estimating rock mass, deformation modulus used the empirical method [34]. The following equation was used:

$$E_{rm} = E_i\left(0.02 + \frac{1 - D/2}{1 + e^{(60+15D-GSI/11)}}\right), \tag{1}$$

where E_{rm} and E_i represent the deformation modulus of the rock mass and the intact rock, respectively.

The following equations were used for the angle of friction (φ) and the cohesive strength (c):

$$\varphi = \sin^{-1}\left[\frac{6am_b\left(s + m_b\sigma_{3n}^1\right)^{a-1}}{2(1+a)(2+a) + 6am_b\left(s + m_b\sigma_{3n}^1\right)^{a-1}}\right],$$
$$c = \frac{\sigma_{ci}\left[(1+a)s + (1-a)m_b\sigma_{3n}^1\right]\left(s + m_b\sigma_{3n}^1\right)^{a-1}}{(1+a)(2+a)\sqrt{1 + 6am_b\left(s + m_b\sigma_{3n}^1\right)^{a-1}/((1+a)(2+a))}}, \tag{2}$$

where m_b, s, and a represent peak strength parameters of Hoek–Brown [32]; σ_{ci}-uniaxial compressive strength of the intact rock; $\sigma_{3n}^1 = \sigma_{3\max}^1/\sigma_{ci}$-the upper limit of confining stress over which the relationship between the Hoek–Brown and the Mohr–Coulomb criteria is considered [32].

The uniaxial compressive strength of the rock mass was calculated as follows:

$$\sigma_{crm} = \sigma_{ci}\, s^a. \tag{3}$$

The tensile strength of the rock mass was calculated as follows:

$$\sigma_{trm} = -\frac{\sigma_{ci}\, s}{m_b}. \tag{4}$$

The properties of the rock mass were calculated for the studied strata. They are listed in Table 1.

According to the classification of the International Society for Rock Mechanics (ISRM), the surrounding rocks were "weak" because their average uniaxial compressive strength (UCS) was in the range of 5–25 MPa [35]. In addition, the surrounding rocks were fissured and wet, and the immediate floor of the roadway was laminated. This explains the large deformations in the roadway. The reliability of ventilation of the 14th eastern panel depends on the deformations degree of the air-return roadway, especially on the rate of floor heave. Therefore, it is imminent to research the control technology of the floor heave.

3. Study of the Floor Heave in Soft Rock

3.1. Numerical Model. The numerical simulation by means of ANSYS was performed to analyze the characteristics of the stress and strain distributions of surrounding rock before and after reinforcing of floor. To simulate the behavior of rock mass, the Drucker–Prager model was used. The model enables simulating plastic deformation of rock and its other pressure-dependent material, which corresponds to the properties of rocks in a fracture zone.

The model simulates a cross-section of roadway with the unit thickness (1 m). The distance between the rows of bolts is 1.0 m. Thus, the support is set in the middle along the thickness of the model (with the coordinate $z = 0.5$). Thus, the condition of symmetry and uniformity is satisfied. When the distance between the rows of anchors is less or more than 1.0 m, then the result obtained should be multiplied by the support density factor $F_d = 1/a$, where a is the actual distance between the rows of anchors.

The numerical model was established according to the actual geological engineering conditions. The model was 1 m long, 60 m wide, and 60 m high. Horizontal displacements were fixed at the lateral boundaries. Vertical displacements were fixed at the bottom boundary. The top boundary was set free. A vertical pressure of 20 MPa, that equivalent to the weight of rocks at a depth of development (800 m), was applied on the top of the model. A 5.5×4.2 m arch shape roadway was adopted, and the beam unit was used to simulate the U-shaped steel support. The filling material (wooden boards) was modeled between rock mass and frames (Figure 5).

For investigation of the evolution on the floor heave of soft rock mass in the deep roadway, the physical and mechanical properties of the rocks were changed during the simulation. This simulated an increase in rock fracturing over time. Numerical accounting of the degree of rock mass discontinuity was carried out by changing the Hoek–Brown parameters: GSI (from 74 to 63) and D (from 0 to 0.7). The initial value of the Hoek–Brown parameters corresponded to the stage of development, and the final state of the parameters corresponded to the roadway reconstruction stage (critical floor heave). The numerical modelling process had 9 steps: 1 step for intact rock and 8 steps for the rock mass. The most detailed was the simulation of the immediate floor, the joint spacing of which was 1.8–0.25 m for steps 2–9, respectively. Properties of the main roof and main floor did not change because these strata were out of the influence of the roadway. Table 2 presents the mechanical parameters of rock mass for each step. The dilatancy angle was taken equal

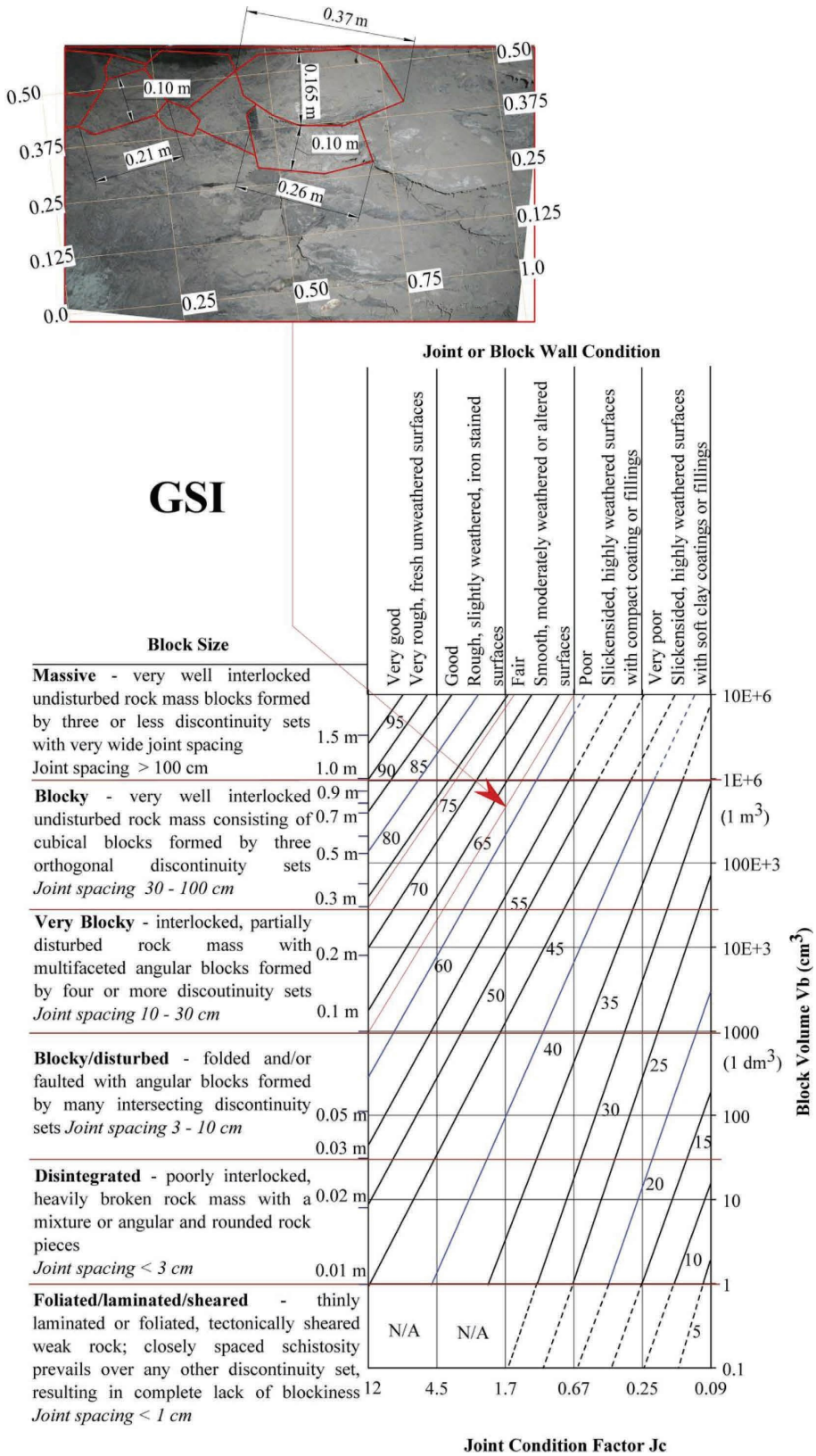

Figure 4: Quantification of GSI chart [33] with indicating region for the studied roadway.

Table 1: Intact rock properties and calculated rock mass properties.

Rock strata	Intact rock			GSI/D/m_i	Rock mass		
	Density (kg/m^3)	Young's modulus (MPa)	Compressive strength (MPa)		Young's modulus (MPa)	Compressive strength (MPa)	Tensile strength (MPa)
During reconstruction of roadway							
Sandy mudstone	2400	3600	40.0	71/0.3/7	2040	6.7	0.55
Sandy mudstone	2400	2245	35.0	67/0.6/7	760	3.5	0.28
Coal C11	1300	1145	9.1	66/0.5/15	420	1.9	0.07
Mudstone	2300	1955	19.3	63/0.7/7	460	1.3	0.10
Sandstone	2400	6120	55.0	72/0.3/7	3573	9.7	0.80
During development of roadway							
Sandy mudstone	2400	3600	40.0	74/0/7	2881	9.4	0.80
Sandy mudstone	2400	2245	35.0	74/0/7	1797	8.3	0.70
Coal C11	1300	1145	9.1	70/0/15	838	3.4	0.12
Mudstone	2300	1955	19.3	73/0/7	1536	4.3	0.36
Sandstone	2400	6120	55.0	74/0/7	4889	13.0	1.20

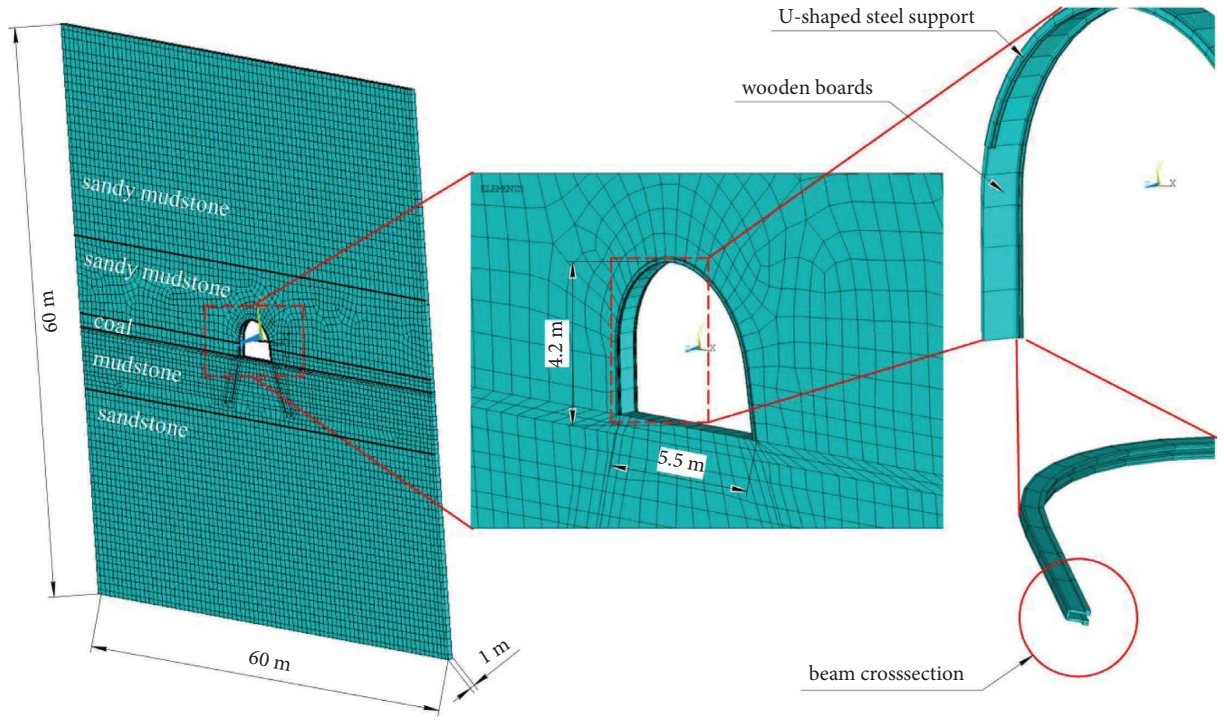

Figure 5: Numerical simulation model and supporting units.

to the angle of internal friction, which corresponded to the unfavorable option. Mechanical parameters of U-shaped steel support are shown in Table 3.

3.2. Simulation Results. The stress distributions of the surrounding rocks are shown in Figure 6. It is seen that the zone of reduced maximum principal stresses σ_1 is formed on the floor of the roadway (Figure 6(a)). In the distance from the floor surface to deep equal to the roadway width, the stress σ_1 is 2-3 times less than out of the roadway influence. The level of tensile stresses near the contour of the floor in the central part of a cross-section of the roadway is greater than the tensile strength of mudstone.

It is the potential zone of rock fracture. This region is highlighted in gray color. On the side of the roadway, the size

Table 2: Rock mass parameters for numerical simulation.

Steps	GSI/ *D*	Compressive strength (MPa)	Tensile strength (MPa)	Deformation modulus (GPa)	Poisson's ratio	Cohesion value (MPa)	Angle of internal friction (deg)	Dilatancy angle (deg)
				Main roof (sandy mudstone)				
1	—	40.0	3.50	3.60	0.3	5.35	30	30
2–9	71/ 0.3	6.7	0.55	2.04	0.3	4.20	28	28
				Immediate roof (sandy mudstone)				
1	—	35.0	3.05	2.24	0.3	6.40	32	32
2	74/0	8.2	0.7	1.79	0.3	5.20	30	30
3	72/ 0.2	6.6	0.54	1.40	0.3	3.30	27	27
4	71/ 0.3	5.8	0.47	1.29	0.3	2.95	26	26
5	70/ 0.4	5.1	0.41	1.09	0.3	2.63	25	25
6	68/ 0.5	4.1	0.35	0.93	0.3	2.37	24	24
7	67/ 0.7	3.5	0.27	0.76	0.3	2.11	23	23
8	67/ 0.7	3.5	0.27	0.76	0.3	2.11	23	23
9	67/ 0.7	3.5	0.27	0.76	0.3	2.11	23	23
				Coal C11				
1	—	9.1	0.10	1.14	0.3	2.60	26	26
2	70/0	3.4	0.12	0.84	0.3	2.30	24	24
3	70/ 0.2	3.0	0.11	0.68	0.3	2.11	23	23
4	69/ 0.3	2.7	0.09	0.60	0.3	1.82	23	23
5	68/ 0.4	2.3	0.08	0.51	0.3	1.64	22	22
6	67/ 0.5	2.0	0.07	0.44	0.3	1.47	21	21
7	66/ 0.5	1.9	0.08	0.42	0.3	1.43	21	21
8	66/ 0.5	1.9	0.08	0.42	0.3	1.43	21	21
9	66/ 0.5	1.9	0.08	0.42	0.3	1.43	21	21
				Immediate floor (mudstone)				
1	—	19.3	1.60	1.80	0.3	4.30	28	28
2	73/0	4.3	0.36	1.53	0.3	3.42	27	27
3	72/ 0.2	3.6	0.30	1.25	0.3	2.89	26	26
4	71/ 0.3	3.2	0.26	1.10	0.3	2.63	25	25
5	70/ 0.4	2.8	0.23	0.96	0.3	2.37	24	24
6	68/ 0.5	2.3	0.18	0.79	0.3	2.11	23	23
7	65/ 0.6	1.7	0.13	0.59	0.3	1.82	23	23
8	64/ 0.7	1.4	0.11	0.50	0.3	1.64	22	22
9	63/ 0.7	1.3	0.10	0.46	0.3	1.47	21	21
				Main floor (sandstone)				
1	—	55.0	3.50	6.12	0.3	19.10	35	35
2–9	72/ 0.3	9.7	0.80	3.50	0.3	5.00	32	32

Table 3: Properties of support elements used in the model.

Primary support	Type of elements	Material behaviour option	Elastic modulus (GPa)	Poisson's ratio	Yield strength (MPa)	Tangent modulus (GPa)
U-shaped steel support	Beam	Bilinear isotropic hardening	200	0.3	342	52.2
Filling material (wooden boards)	Solid	Isotropic	750	0.3	—	—

of the zone of reduced σ_1 reaches half the roadway width. An insignificant decrease in stresses also occurs in the roof of the roadway.

The analysis of the distribution patterns of the minimum principal stresses σ_3 (Figure 6(b)) shows that an area of increased σ_3 is formed on the sides of the roadway in the distance from the side wall surface to the deep equal to the roadway width. The largest σ_3 are formed at the bottom corners of the roadway.

After the development of the roadway, deformations of the roof, side wall, and floor are not large. The distribution of vertical displacement of the roof and floor after development is shown in Figure 6(c). The floor heave of the roadway is 0.072 m. The roof subsidence is 0.03 m. Maximum principal strains of surrounding rocks are within the limits of elasticity, except for the bottom corners of the roadway (Figure 6(d)).

The results of laboratory tests show that the failure strain of mudstone is 0.018–0.02, and of the coal is 0.012–0.016 (Figure 3). This corresponds with the results of testing soft rock specimens in a volumetric field [36–38] and under uniaxial compression [39, 40]. According to the results of tests, it was found that for mudstone, siltstone, argillite, and sandstone with uniaxial strength of 25–40 MPa, the failure criteria for strain is about 0.02-0.03. Thus, for this study, the failure limit is in the range of "−0.02"–"+0.02".

Figure 7 shows the distributions of minimum principle stress (σ_3) around the roadway in the simulation increasing in rock fracturing. The evolution of σ_3 shows that on the roof and on the floor of the roadway the reduced stress areas increase step by step. At the same time, roof subsidence occurs, and floor heave grows. The σ_3 in the bottom corners of the roadway significantly exceed the compressive strength of the mudstone. Under the foot of the arch support, there is a high probability of rock destruction.

The size of the increased σ_3 zone on the side wall increases. So the width of the increased stress zone, in which σ_3 is 5–30% greater than σ_3 before excavation, exceeded the width of the roadway (W) at the last step of the simulation by 1.5 times. Near the contour of the roadway, the nature of the stress changes significantly. The monitoring line A-A^1 was arranged along the horizontal axis, and the stress on this line changed with the number of calculation steps (Figure 8(a)). Figure 8(a) shows that at 2, 3, and 4 steps in the near-contour area with a depth of 0.7 m, a decrease in stresses is observed; however, at subsequent steps, stresses increase in this area. This can be explained by the compression of rocks near the contour of the roadway, caused by the resistance of the frame support, which increases with the increasing displacement of rocks.

The stress concentration factor is defined as the stress value at that point divided by the stress before excavation. For simulation steps, 2 and 9 the stress concentration factor on the right side of the roadway is presented in (Figure 8(b)). It is observed that σ_3 concentrates on the roadway sides at a depth of 1.2 m, with a stress concentration factor of 1.16. With an increase in the number of calculation steps, the σ_3 concentration factor continuously increases, and the concentration of stress shifts to the deep part. At the last simulation step, σ_3 concentrates at the depth of 1.8 m, with a stress concentration factor of 1.19.

Figures 9 and 10 show the distributions of maximum principle stress and maximum principle strain, respectively, for the surrounding rocks with calculation steps. Figure 9 shows that the size of the reduced stress zone in the floor and the roof of the roadway with an increase in the number of calculation steps increases gradually. Thus, the size of the reduced stress zone, in which σ_1 is 2.8 times less than before excavation, increases from 0.68 W to 1.0 W. At the same time, as the reduced stress zone in the floor increases, on the wall sides of the roadway, the stresses become less intense. The size of the reduced stress zone with an increase in the number of calculation steps increases.

The σ_1 in the central part of the roadway floor significantly exceed the mudstone tensile strength, which indicates a high probability of rock failure. Obviously, the evolution of σ_1 correlates with the growth of the floor heave.

The maximum principle strain of surrounding rocks of the roadway is increased nonlinearly with an increase in the number of calculation steps, as shown in Figure 10.

The maximum principle strains in the immediate floor exceed the failure limit (+0.02). This indicates the formation of cracks in the floor. Initially, post-peak strain regions appear in the bottom corners of the roadway, after which they develop into the depths. In this way, strata on the immediate floor are destroyed one by one, starting from the corners of the roadway. At the 6th simulation step, these regions merge in the roadway floor at a depth of about 2.0 m, forming a closed contour. The gray color in Figure 10 highlights the regions of rocks in which the maximum principle strain is 2.5 times greater than the post-peak ones. It can be seen that at the 9th step, the strata on the immediate floor to a depth of more than 2.0 m are included in this region. Thus, a high degree of floor destruction is evident there. Dilatancy and plastic flow of rocks are observed in this region, which causes significant floor heave.

Figure 11 shows the floor heave on monitoring line B-B^1 and vertical plastic strain distribution at 1, 6, 8, and 9 steps. Post-peak plastic strains appear at the 6th simulation step. The nonlinear nature of floor heave is clearly seen in the

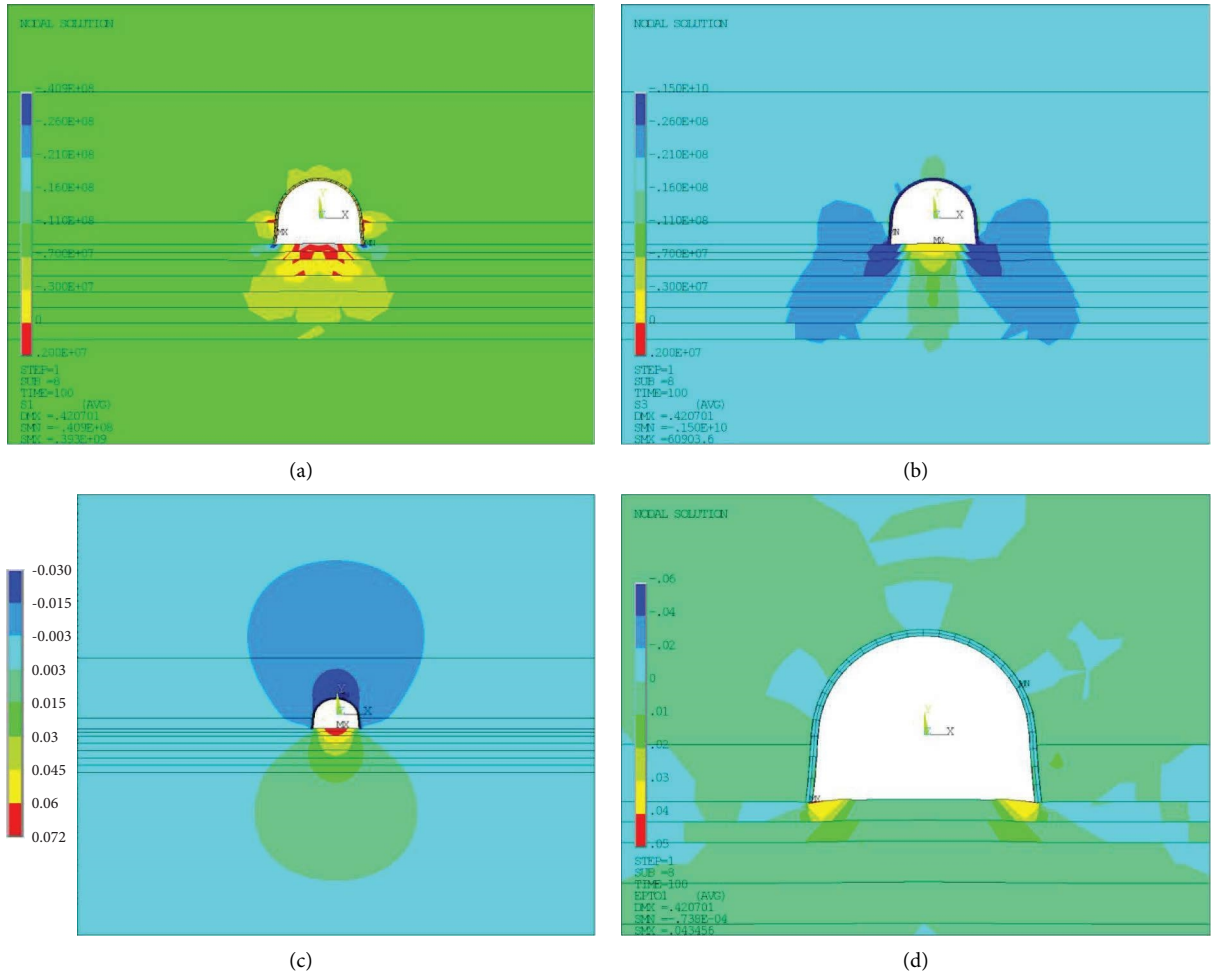

Figure 6: The results of numerical calculation in the case of roadway development: (a) distribution of maximum (σ_1) principal stresses; (b) distribution of minimum (σ_3) principal stresses; (c) distribution of vertical displacement; (d) distribution of maximum principal strains.

graphs in Figure 11. Thus, the nonlinear increase in heaving is a consequence of the transition of rocks to the stage of plastic deformation.

3.3. Simulation Discussions. Several conclusions can be drawn according to the above analyses:

(1) The roof and side walls were controlled adequately by the original steel arch support. In this, the simulation results correspond with observations of the roadway in situ.

(2) The stress analysis shows that with an increase in rock mass fracturing (number of calculation steps), the σ_3 concentration factor on the side wall of the roadway continuously increases, and the concentration of stress shifts to the deep rock mass part. The σ_3 in the bottom corners of the roadway significantly exceed the compressive strength of the immediate floor, which indicates a high probability of rock cracking under the foot of the arch support. At the same time, the size of the reduced σ_1 stress zone in the floor and the roof of the roadway increases gradually. The σ_1 in the central part of the roadway floor significantly exceed the tensile strength of the immediate floor, which indicates a high probability of rock crushing.

(3) The strain analysis shows that the size of the post-peak maximum principle strain zone in the floor and side wall of the roadway increases nonlinearly with an increase in rock mass fracturing (number of calculation steps). The analysis shows that a significant proportion of maximum principle strains are plastic strains. They exceed the failure limit more than 2.5 times and cause the floor heave. Initially, post-peak strain regions appear in the bottom corners of the roadway, after which strata in the immediate floor are destroyed one by one, into the depth. After that post-peak strain regions merge in the central part of the roadway floor at a depth of about 2.0 m. Finally, the strata in the immediate floor to a depth near 2.0 m are included in the post-peak strain region, which indicates a high probability of rock crushing. This region of the surrounding rocks is mainly involved in the development of floor heave.

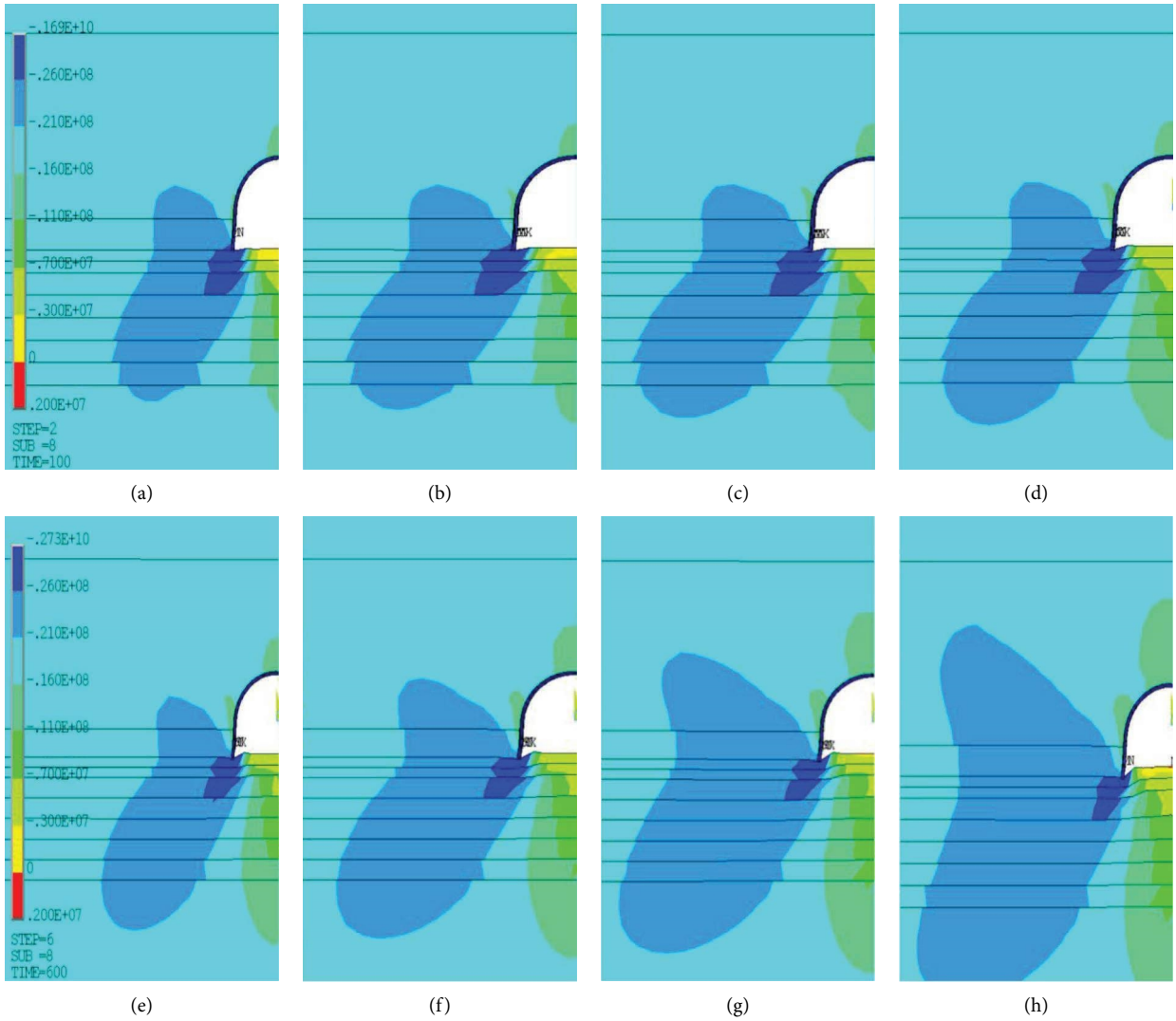

Figure 7: Minimum principle stress (σ_3) distribution around the roadway with a step-by-step increase in rock fracturing: (a) step 2; (b) step 3; (c) step 4; (d) step 5; (e) step 6; (f) step 7; (g) step 8; (h) step 9.

Dilatancy and plastic flow of rocks are observed in this region, which causes significant floor heave.

(4) The key to floor heaving control is to control the development of the crushing zone on the immediate floor. It is necessary to limit the development of post-peak strains from the bottom corners of the roadway deep into the massif and prevent their merging on the immediate floor. This will limit plastic deformations and dilatancy in the immediate floor, which will have a positive effect on the floor heave intensity. The critical is the 6th simulation step, which corresponds to an average joint spacing of 0.45 m in the immediate floor, as shown in Figure 12. After the merging of the post-peak strain regions and the formation of a closed contour in the immediate floor by them (simulation step 7), the heaving growth acquires an obvious nonlinear character. At this step, significant plastic deformation begins, which is the cause of uncontrolled floor heave.

4. Floor Heave Control Technology

Based on the above analysis results, the rock bolts reinforcement was proposed for the floor heave control. This technology has been widely applied in mining. Taking into account the evolution of stresses and strain in the floor of the roadway, the proposed support method should include optimal bolt parameters and arrangement.

4.1. Design of Floor Heave Control Scheme. The region of critical stress and post-peak strain in the immediate floor is limited to a depth of 2.25 m. Three rock bolt arrangements were proposed in which the orientation of the bolts was varied. Fully grouted resin bolts were used. In modelling, the length of the bolts was different for different schemes. At the same time, the bolts lengths were assumed to multiple ones to the length of the reinforcement zone: 5 m; 4 m; 3 m; 2 m; and 1 m. When the anchoring depth was significant, the bolts consisted of sections.

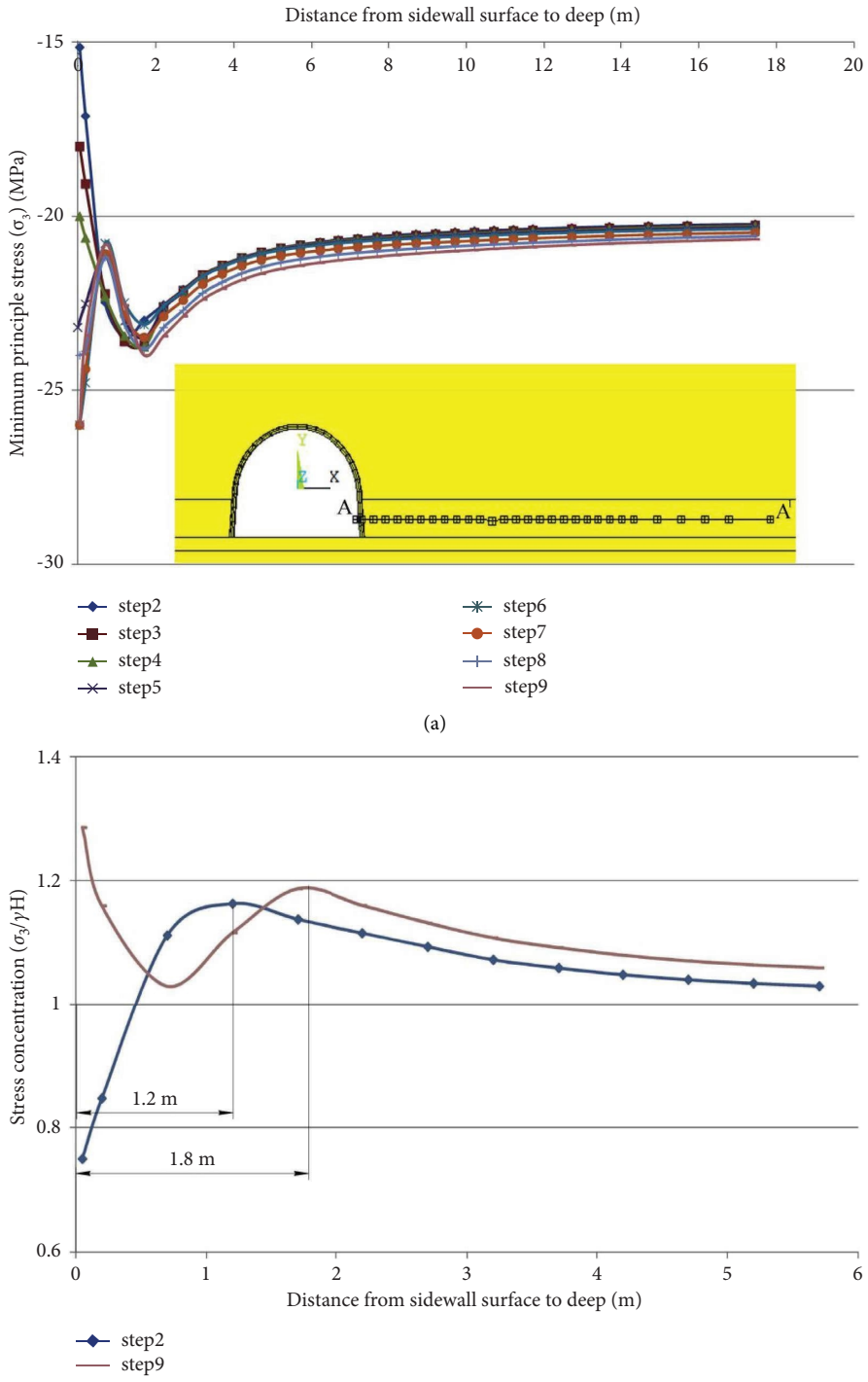

Figure 8: (a) Characteristics of minimum principle stress (σ_3) on monitoring line A-A^1 with calculation steps; (b) characteristics of stress concentration factor ($\sigma_3/\gamma H$) on monitoring line A-A^1 for steps 2 and 9.

The maximum length of the bolts was limited by the strata level $L_{max} = 5.0$ m. The bolts with traditional bearing plates were used firstl, and then bolts with steel belts were used. The original U-shaped steel support was still unchanged. Table 4 shows the setting of mechanical parameters of the rock bolts and other supporting components in the numerical model.

Figure 13 shows the support schemes of the roadway with the rock bolts reinforcement. The optimal floor heave control scheme provides an acceptable floor heave with a minimum rock bolt length. The floor support elements that were used in the model are shown in Figure 14.

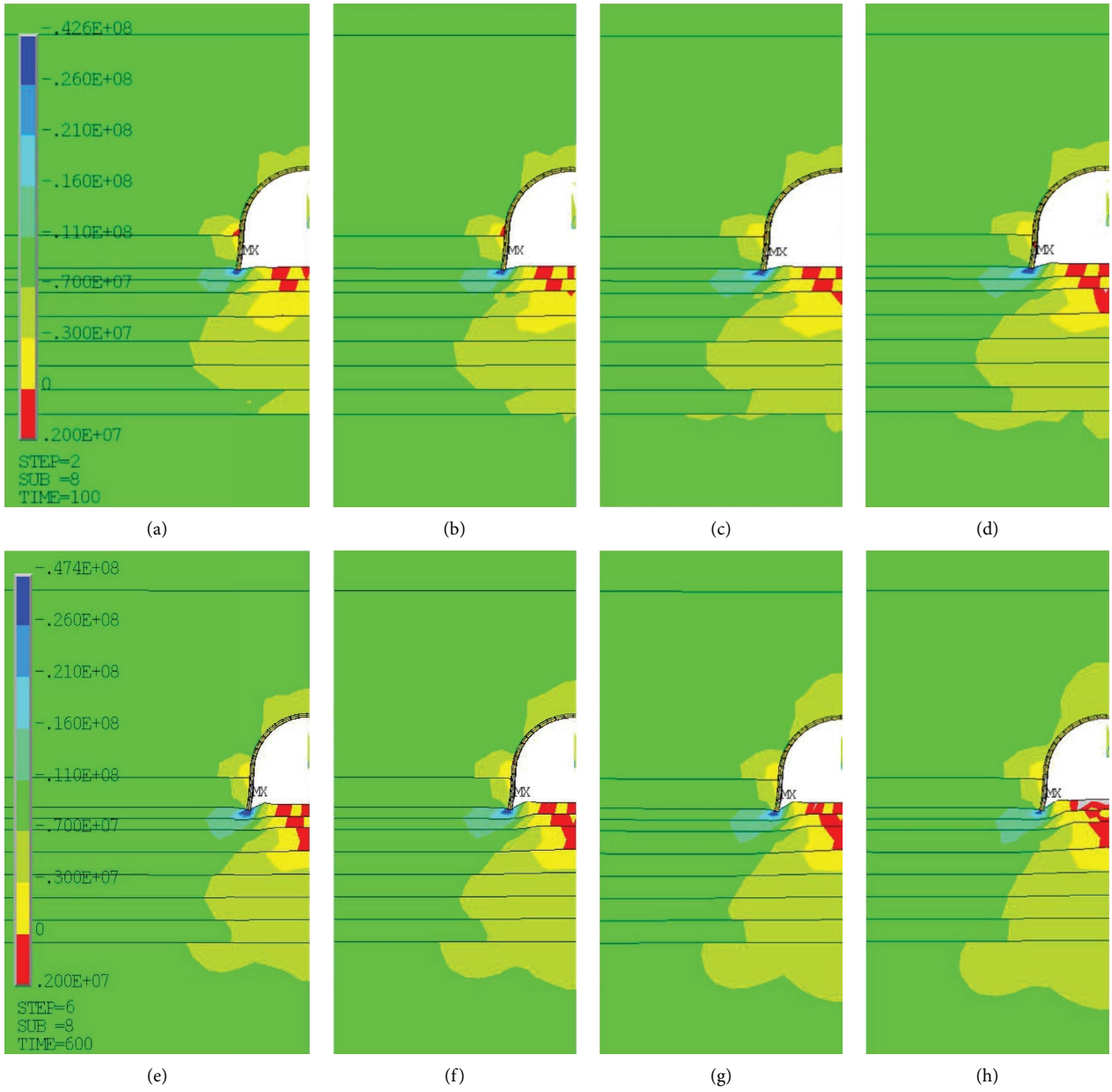

Figure 9: Maximum principle stress (σ_1) distribution around the roadway with a step-by-step increase in rock fracturing: (a) step 2; (b) step 3; (c) step 4; (d) step 5; (e) step 6; (f) step 7; (g) step 8; (h) step 9.

4.2. Effectiveness of Rock Bolts Reinforcement. Firstly rock bolts with bearing plates were modeled. Although the minimum principal stress in rock bolts and in the frame is less than the tensile strength of steel, the loading results in significant deformation of the frame and bolts, as shown in Figure 15(a). Most of all, the rock bolts located at the edges are bent. The analysis of vertical strains shows that the installation of bolts without additional elements generally has a positive effect on the heaving intensity. However, with this variant of floor support, post-peak strains are observed near the corners of the roadway in the near-contour of the immediate floor, as shown in Figure 15(b). This reduces the effectiveness of the reinforcement and can lead to further development of rock crushing on the immediate floor. As an element of coupling steel belt was proposed across the entire width of the roadway's floor. A comparison of the effectiveness of floor support by bolts with steel belts and without it was made for the last simulation step, which corresponds to an average joint spacing of 0.10 m in the immediate floor.

Figure 16 shows the distributions of maximum principle stress for the surrounding rocks at the last simulation step after reinforcement for different floor support schemes. The zone of reduced stress σ_1 in the roadway floor as a result of rock bolts reinforcement is reduced in size compared to the case without reinforcement (Figure 9(h)). However, near the contour of the roadway in the immediate floor, σ_1 are formed that exceed the tensile strength of rock. The regions of critical σ_1 are located between the rock bolts. In the case of

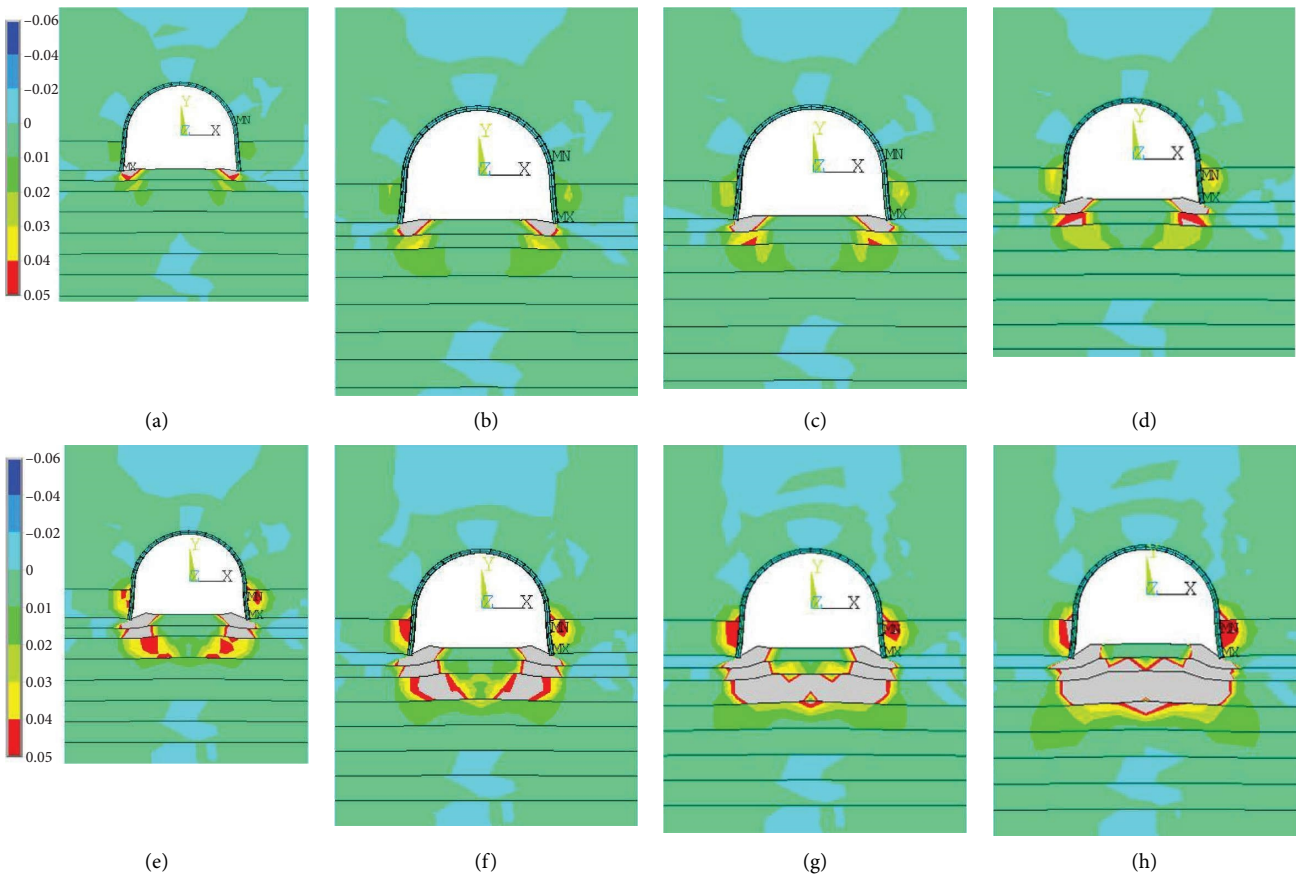

Figure 10: Total maximum principle strain distribution around the roadway with a step-by-step increase in rock fracturing: (a) step 2; (b) step 3; (c) step 4; (d) step 5; (e) step 6; (f) step 7; (g) step 8; (h) step 9.

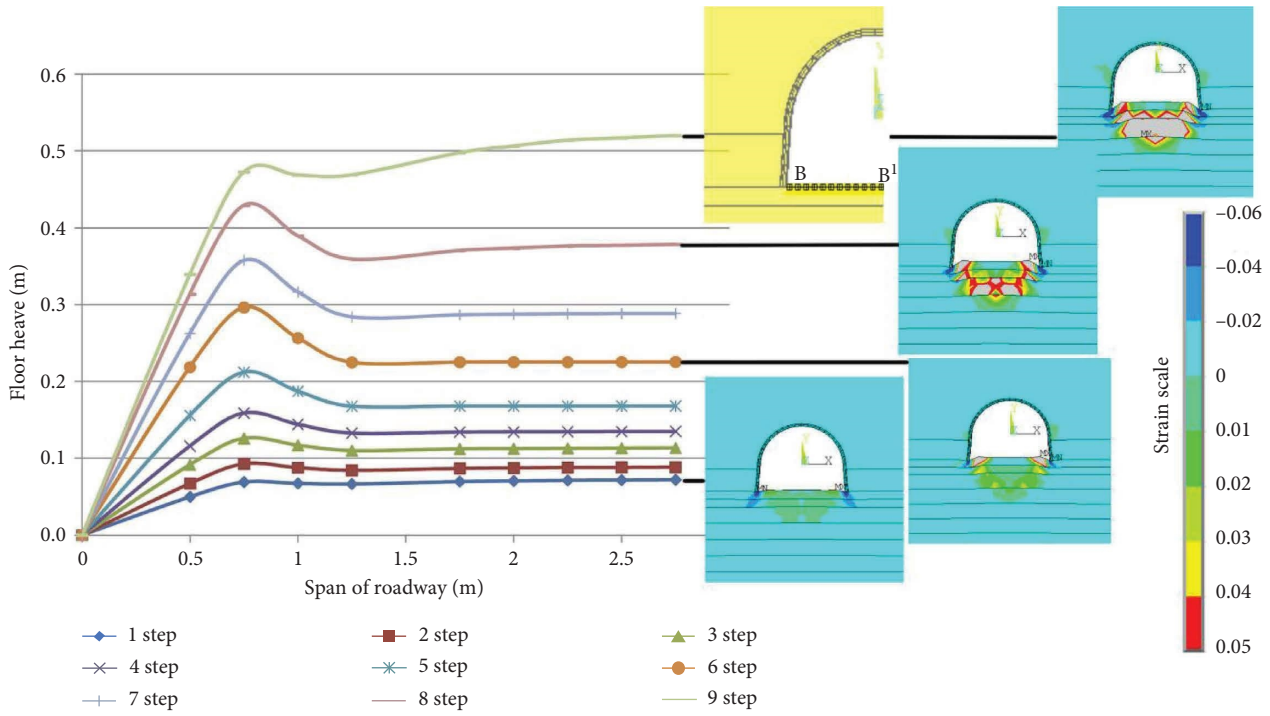

Figure 11: Floor heave on monitoring line B-B^1 and vertical plastic strain distribution around the roadway.

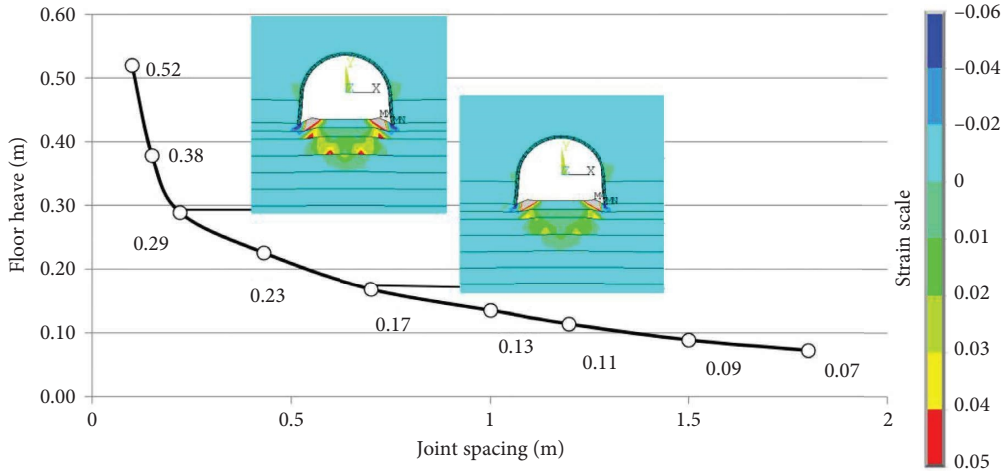

Figure 12: The relationship between joint spacing in the immediate floor and floor heave and vertical plastic strain distribution around the roadway for steps 5 and 7.

Table 4: Properties of floor support elements used in the model.

Floor support element	Cross-sectional area (m^2)	Material behaviour option	Elastic modulus (GPa)	Poisson's ratio	Yield s/trength (MPa)	Tangent modulus (GPa)
Bolt	8.04×10^{-4}	Bilinear isotropic hardening	200	0.3	342	52.2
Steel belt	7.5×10^{-4}	Isotropic	200	0.3	—	—

using rock bolts with steel belts, such regions do not occur, the zone of reduced stress is smaller, and the contour of the roadway floor is smoother. There is also a tendency to change the size of the zone of reduced stress σ_1 with a change in the installation angle of rock bolts. The maximum vertical sizes of this zone are formed at support scheme I and the minimum ones are formed at support scheme III. This is true both for the case of bolts without steel belts and for the case with steel belt. The analysis of Figure 16 gives grounds to believe that the presence of a steel belt in the floor support system leads to a change in the distribution of stress on the immediate floor.

Figure 17 shows the distribution of maximum principle strain for the surrounding rocks before and after reinforcement with different support elements for support scheme II. The analysis of the figure helps to trace the influence of each floor support element on the distribution of strain on the immediate floor. The installation of a steel belt without rock bolts makes it possible to reduce the size of the post-peak strain region in the roadway floor, as shown in Figure 17(b). At the same time, the contour of the floor in the bottom corners of the roadway is smoothed out. However, a zone of immediate floor to a depth of about 2.0 m is still in the region where the strains exceed the post-peak ones by more than 2.5 times. Thus, the destruction of the immediate floor is very probable, and the effectiveness of such reinforcement is low.

The installation of rock bolts without a steel belt significantly changes the size and shape of the post-peak strain regions, as shown in Figure 17(c). These regions are located under the bottom corners of the roadway along the rock bolts and no longer form a closed contour. The total value of floor heave is reduced. The coupled use of rock bolts with a steel belt reduces the size of the region with a post-peak strain by 1.5 times compared to the case without the steel belt. The optimal effect of such reinforcement is obvious, as shown in Figure 17(d).

Figure 18 shows the floor heave on monitoring line B-B^1 and vertical plastic strain distribution around the roadway before and after reinforcement with different supporting elements for floor support scheme III. The roadway support is symmetrical about the axis of its cross-section, so the graphs in Figure 18 are shown only half of the roadway span. Analysis of the figure makes it possible to track the proportion of the contribution of each supporting element to the decrease of floor heave. The installation of a steel belt without rock bolts reduces floor heave by 17% while smoothing it out in the bottom corners of the roadway. At the same time, the region of post-peak vertical plastic strain is formed on the immediate floor. Reinforcement by rock bolts without a steel belt reduces floor heave by 44%. However, in the bottom corners of the roadway, vertical plastic strain forms regions with a depth of 0.5 m in which the strain is more than 2.5 times than the post-peak one. The destruction of rocks in these regions is highly probable, which reduces the effectiveness of reinforcement in the future. In the case of coupled use of rock bolts with steel belt, the total value of floor heave is reduced by 48%, and post-peak vertical strain is not formed in the near-contour area. Still, there are insignificant regions of post-peak vertical strains under the legs of the frame. However, the sizes of these

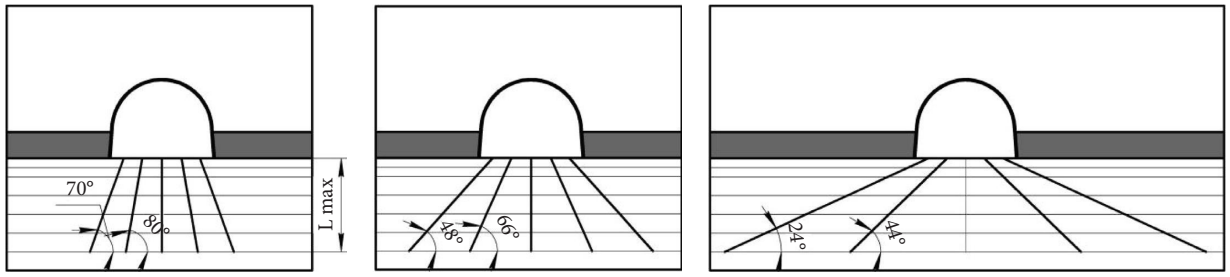

Figure 13: The floor support schemes with different bolt orientations: (a) scheme I; (b) scheme II; (c) scheme III.

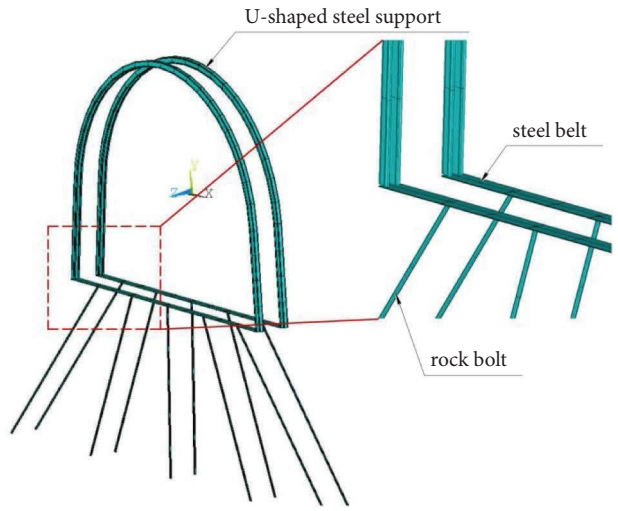

Figure 14: Support elements in the numerical model.

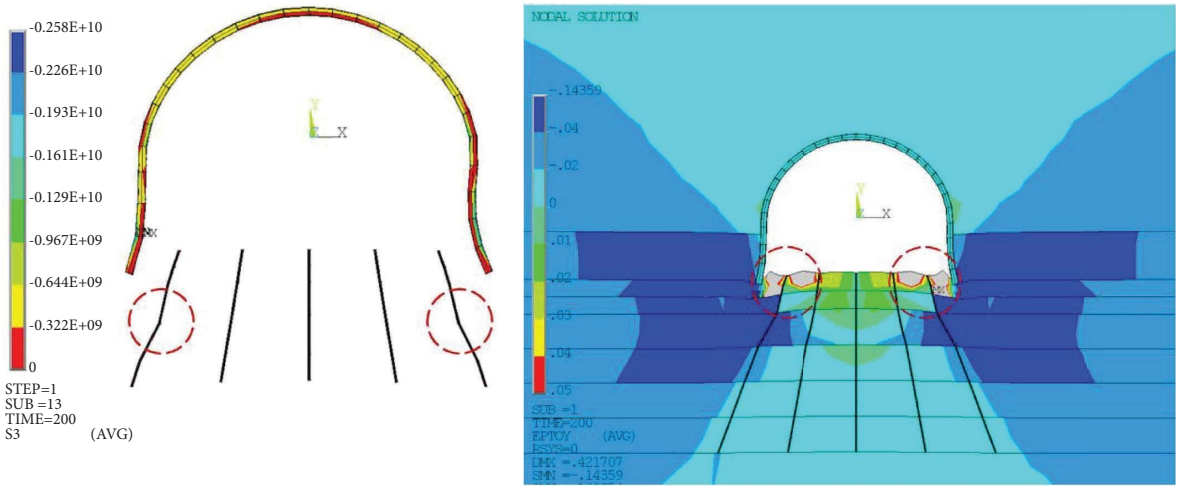

Figure 15: (a) Minimum principle stress (σ_3) distribution in support elements; (b) vertical total strain distribution around the roadway.

regions and, accordingly, the cracking floor rocks are noticeably lower than in other cases. Thus, it is obvious that the best floor supporting effect is in the case of coupled installation of rock bolts with a steel belt. The absence of a steel belt reduces the effectiveness of floor stabilization.

The most effective floor heave support scheme should provide the maximum bearing capacity of the rocks. Rock bolt arrangement highly influences the maximum principle strain distribution around the roadway, as shown in Figure 19. Reducing the angles of the bolts leads to a decrease in the size of the post-peak strain region in the roadway floor.

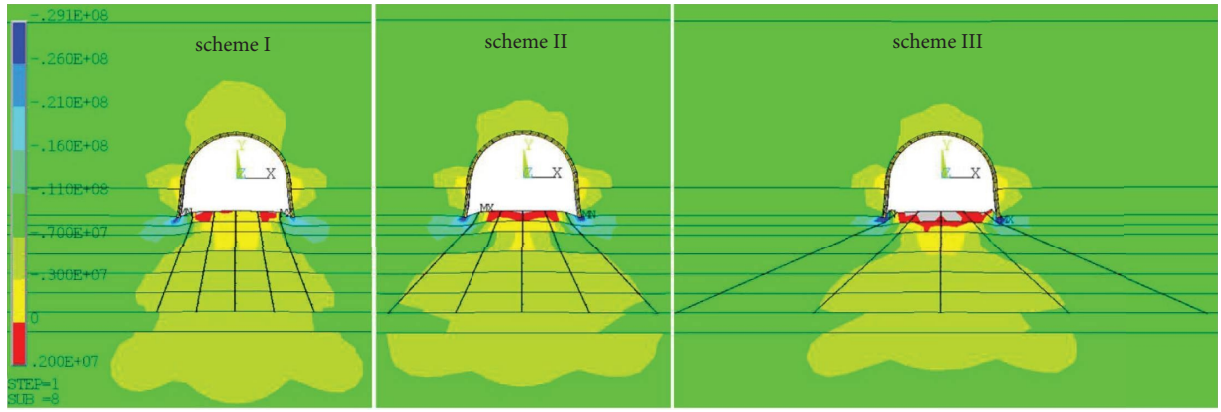

(a)

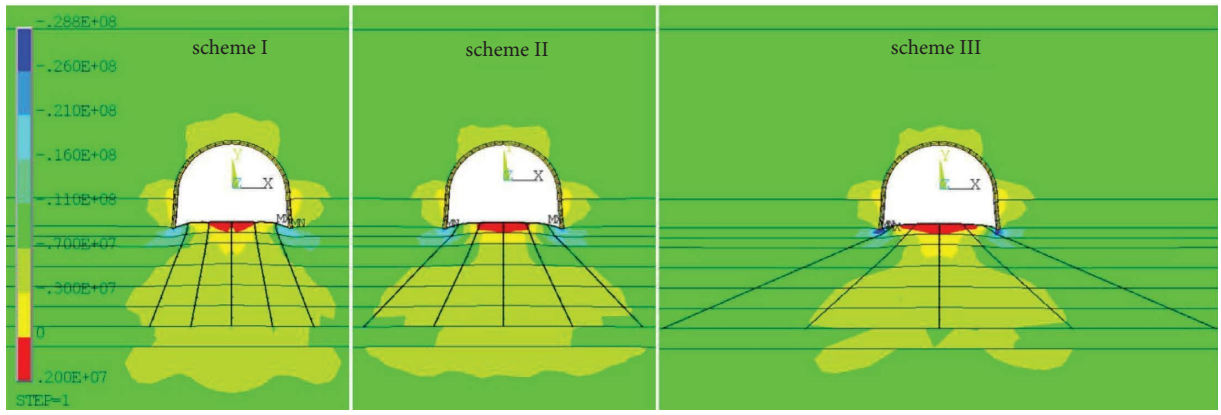

(b)

Figure 16: Maximum principle stress distribution around the roadway after floor bolting: (a) rock bolts without additional supporting elements; (b) rock bolts with steel belt.

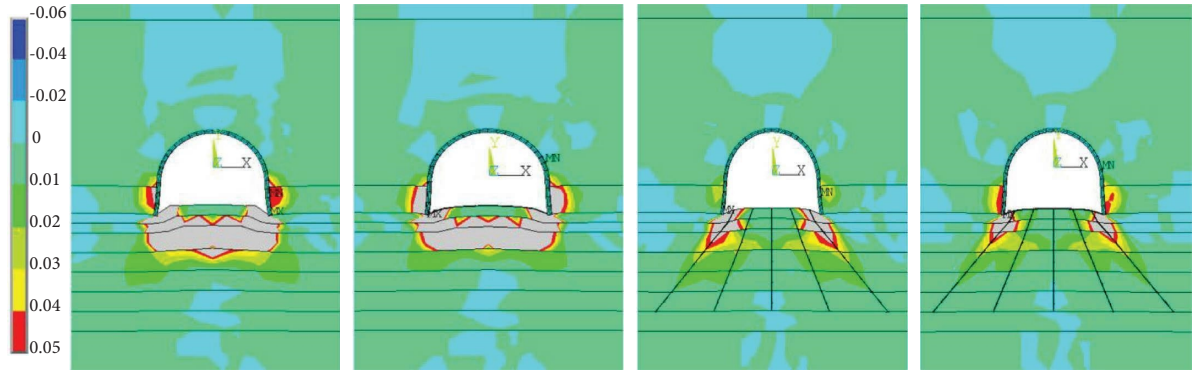

(a) (b) (c) (d)

Figure 17: Total maximum principle strain distribution around the roadway: (a) without floor support; (b) with steel belt; (c) with rock bolts; (d) with rock bolts and steel belt.

The best floor support scheme is scheme III, in which the region of post-peak maximum principle strain, which is highlighted in Figure 19 with gray color, is much smaller than in other cases.

This conclusion is also confirmed by the maximum decrease of floor heave in scheme III, as shown in Figure 20. Although the difference in the value of floor heave between different schemes is insignificant, the distribution of vertical plastic deformation confirms that scheme III is more efficient. Thus, in the case of using scheme I in the near-contour area in the corners of the roadway, both post-peak plastic strains of compression and tension appear, which can serve as an indicator of crack and crash rocks. With scheme II, post-peak plastic compressive strains are formed under the legs of the frame. In the case of using scheme III, only very small regions of post-peak

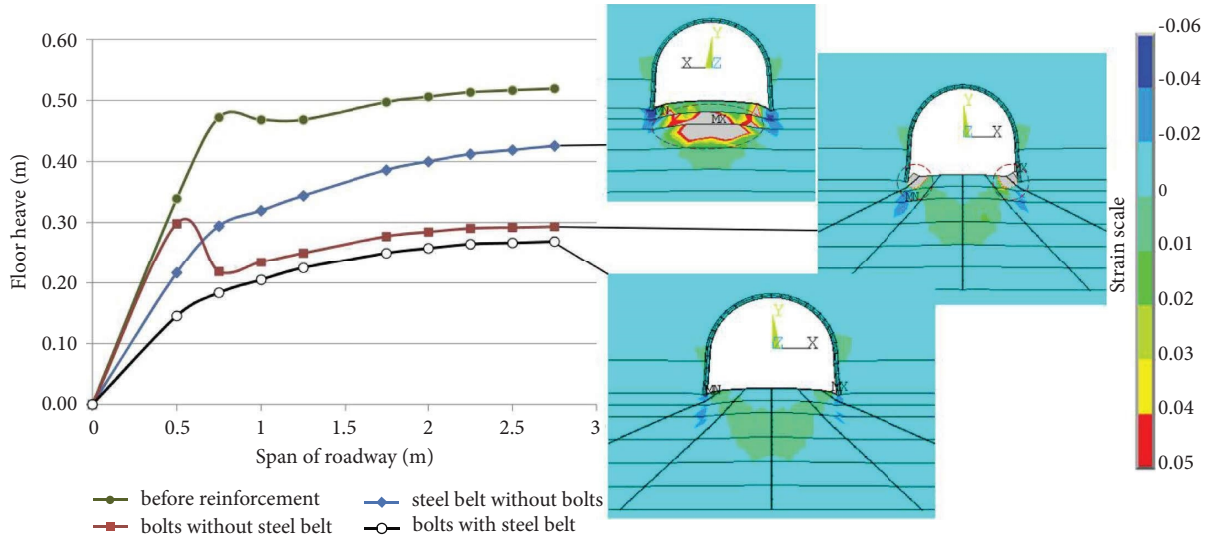

FIGURE 18: Floor heave on monitoring line B-B[1] and vertical plastic strain distribution around the roadway before and after reinforcement with different support elements (floor support scheme III).

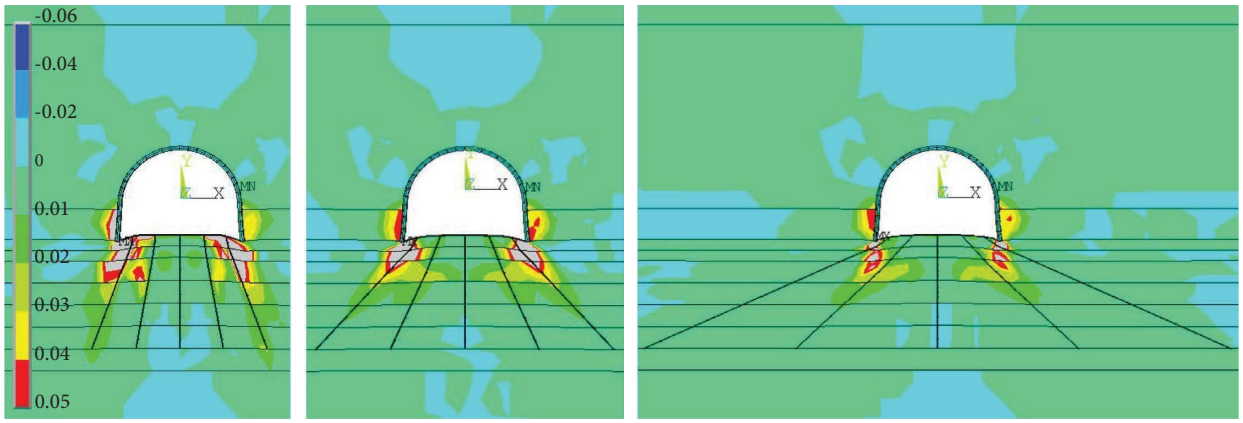

FIGURE 19: Total maximum principle strain distribution around the roadway after reinforcement: (a) floor support scheme I; (b) floor support scheme II; (c) floor support scheme III.

compressive strains are formed. Obviously, scheme III is the most effective for floor support.

During the simulation, the immediate floor was reinforced to a depth of 1.0 to 5.0 m. This made it possible to determine the optimal length of the rock bolts. The corresponding simulation results for floor support scheme III are shown in Figures 21 and 22.

As shown in Figure 21, the reduction of the reinforced zone size (L_r) from 5.0 to 2.0 m does not significantly affect the distribution of the total maximum principle strain. The sizes and configuration of the regions of post-peak strain in the roadway floor are almost unchanged. When L_r is reduced to 1.0 m, the pattern of strain distribution noticeably changes. The regions of post-peak strain increase significantly in size. At the same time, post-peak strains exceed the limits by more than 2.5 times. These regions merge in the central part of the roadway floor. Thus, the zone of the probable crash of rocks has a closed contour. Dilatancy and plastic flow of rocks are observed below the reinforcement length. These processes lead to intense floor heave. Their development will reduce the effectiveness of reinforcement in the future. A significant increase in floor heave with a decrease in L_r from 2.0 to 1.0 m is also noted on the floor heave curve, as shown in Figure 22. In the case when L_r has a size from 5.0 to 2.0 m the floor heave does not change significantly, the results are within the accuracy of the calculations. Taking into account the margin of safety, it was proposed to limit the length of the outer bolts with a reinforcing depth of 2.0 m and the length of the central bolts with a depth of 3.0 m. The total maximum principle strain distribution around the roadway is shown in Figure 22.

4.3. Support Scheme of the Surrounding Rock. Through field observations and numerical calculations, it became clear that the current support system cannot maintain the stability of the surrounding rocks, especially of the immediate floor. The original support method must be improved and optimized. Based on the analysis of the literature review and results of

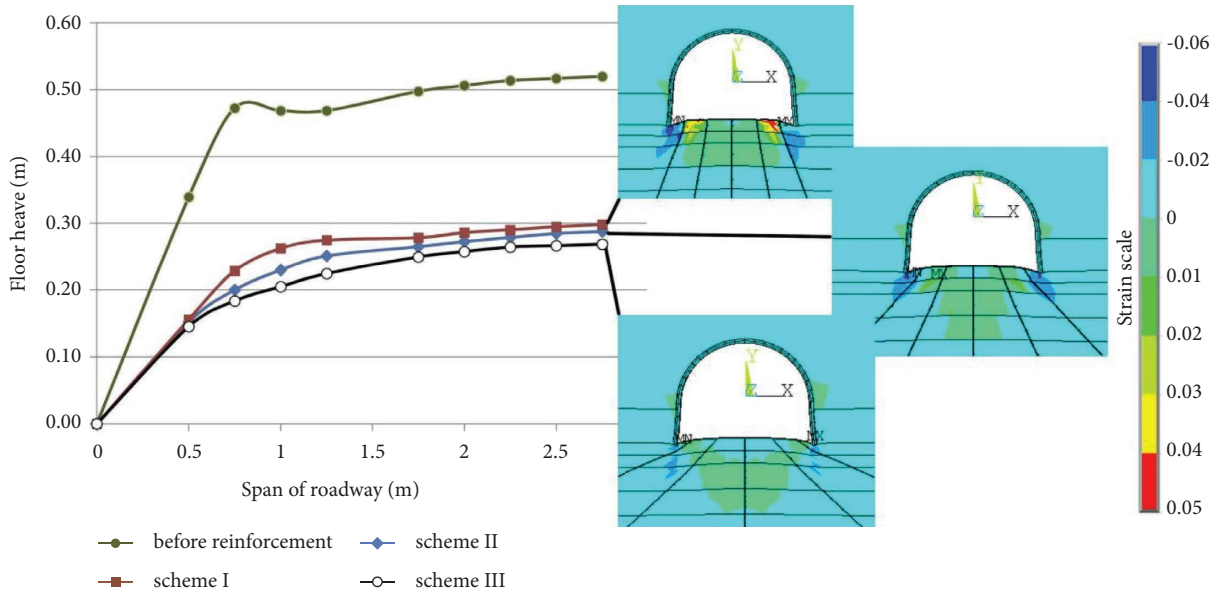

FIGURE 20: Floor heave on monitoring line B-B[1] and vertical plastic strain distribution around the roadway before and after reinforcement with different floor support schemes.

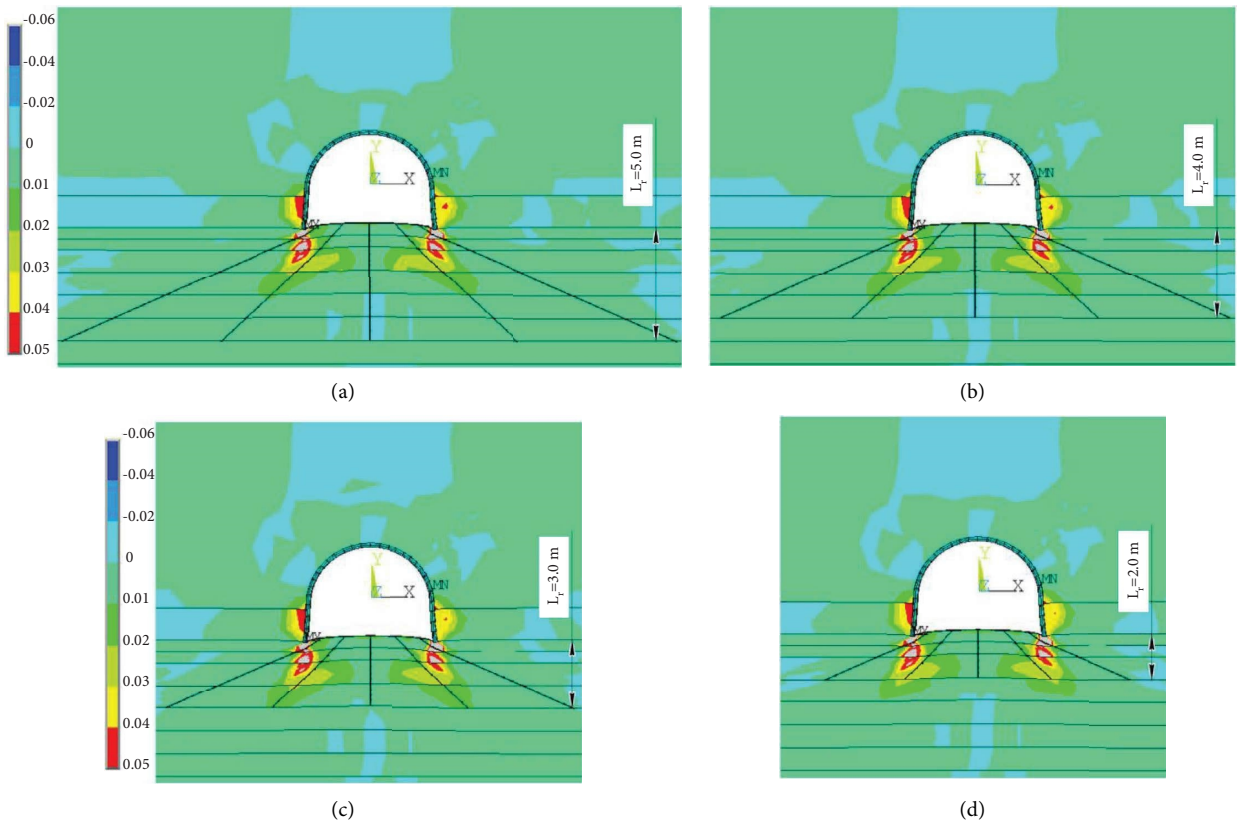

FIGURE 21: Continued.

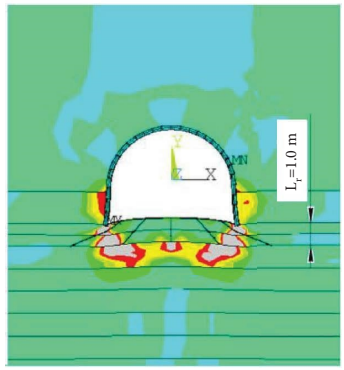

(e)

Figure 21: Total maximum principle strain distribution around the roadway after floor supporting with different lengths of reinforcement (L_r): (a) 5 m; (b) 4 m; (c) 3 m; (d) 2 m; (e) 1 m.

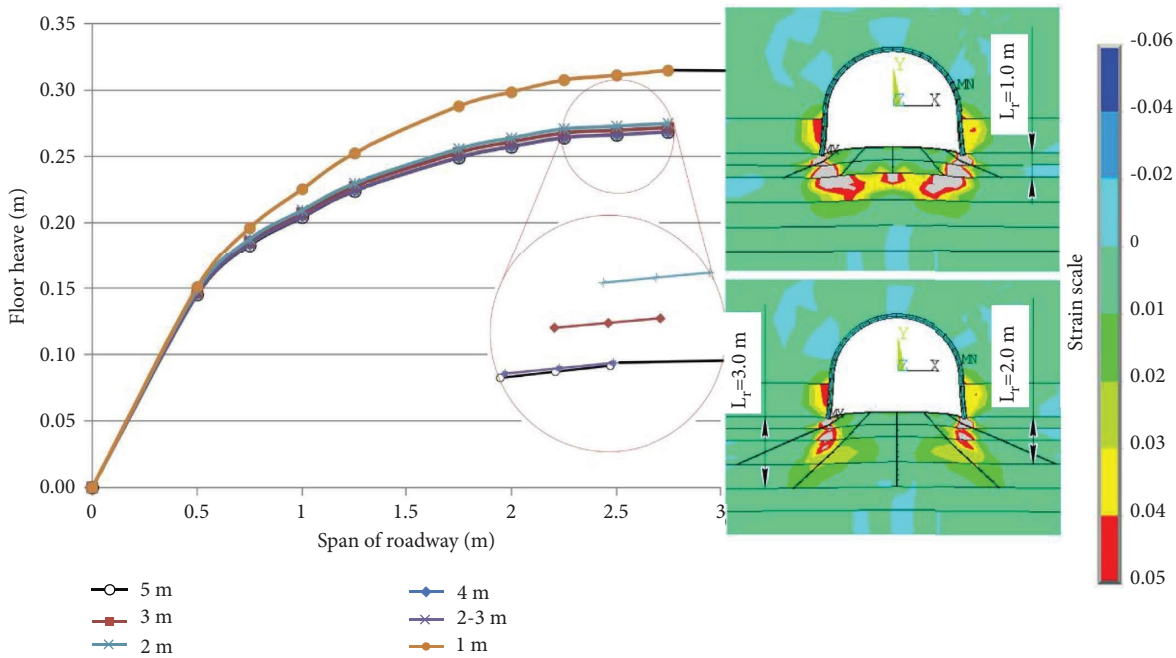

Figure 22: Floor heave on monitoring line B-B[1] (Figure 11) and total maximum principle strain distribution around the roadway after floor supporting with different lengths of reinforcement.

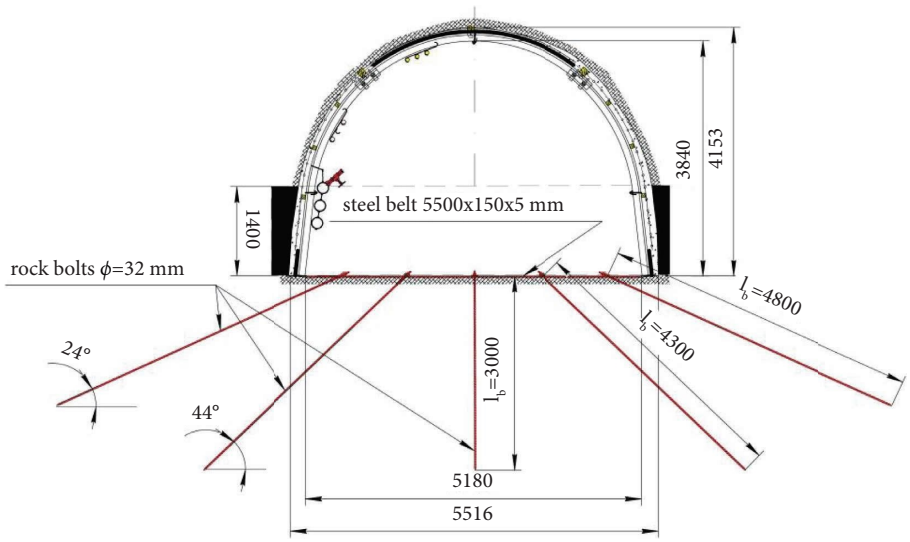

Figure 23: Design of support scheme.

numerical simulation, the rock bolts reinforcement was proposed for the floor heave control. Based on the results of the numerical simulation, the most effective floor support scheme was proposed, and the optimal bolt length is justified. Figure 23 shows the proposed design of the support scheme.

5. Conclusions

In this study, deep mining roadway in soft rock was considered as the research subject. We focused on the floor heave evolution and the effectiveness of rock bolts reinforcement of the roadway. A numerical simulation was used to study the stress-strain state and displacement of surrounding rocks in the underground coal mine 800 m in the depth of Ukraine. The results demonstrated that significant floor heavecaused nonlinear deformation of the laminated immediate floor under an increase in rock fracturing. This was followed by investigating the effectiveness of rock bolts reinforcement. Based on the results of this investigation, the following conclusions can be drawn:

(1) The numerical analysis shows that with an increase in rock mass fracturing, the σ_3 in the bottom corners of the roadway significantly exceed the compressive strength of the immediate floor, which indicates a high probability of rock cracking under the foot of the arch support. The σ_1 in the central part of the roadway floor significantly exceed the tensile strength of the immediate floor, which indicates a high probability of rock crushing. At the same time, the size of the reduced σ_1 stress zone in the floor of the roadway increases gradually. The size of post-peak maximum principle strain regions in the floor of the roadway is increased nonlinearly with an increase in rock mass fracturing. The analysis shows that a significant proportion of maximum principle strains are plastic ones. They exceed the failure limit more than 2.5 times and cause the floor heave.

(2) Initially, post-peak strain regions appear in the bottom corners of the roadway, after which strata in the immediate floor are destroyed one by one into the depth. After that, post-peak strain regions merge in the central part of the roadway floor at a depth of about 2.0 m. Finally, the strata in the immediate floor to a depth near 2.0 m are included in the post-peak strain region, which indicates a high probability of rock crushing. This region of the surrounding rocks is mainly involved in the development of floor heave. The joint spacing of 0.45 m on the immediate floor is critical. At this step, significant plastic deformation begins, which is the cause of uncontrolled floor heave.

(3) Considering the floor heave mechanism of the soft rock, rock bolts reinforcement was proposed to control the floor heave. Three floor support schemes with two types of support elements, different bolt orientations, and lengths of reinforcement were studied during many numerical simulations. After reinforcement, post-peak plastic strain in the floor strata was reduced effectively. The optimal floor support scheme and depth of reinforcement were determined by the allowable floor heave. Ideally, the floor heaves could be reduced by rock bolts with steel belts installed according to the support scheme III and reinforcement length of 2.0 m for outer bolts and 3.0 m for central bolts. This can provide suggestions for the specific parameters suitable for controlling the floor heave of the roadway through rock bolts reinforcement technology.

Data Availability

The data of numerical simulation in ANSYS that were used to support the findings of this study are available from the corresponding author upon request.

Conflicts of Interest

The authors declare that they have no conflicts of interest.

References

[1] F. Zhang, J. Liu, X. Zhang, H. Ni, and Y. Liu, "Research on excavation and stability of deep high stress chamber group: a case study of Anju Coal Mine," *Geotechnical & Geological Engineering*, vol. 39, no. 5, pp. 3611–3626, 2021.

[2] J. C. Chang, D. Li, T. F. Xie, W. B. Shi, and K. He, "Deformation and failure characteristics and control technology of roadway surrounding rock in deep coal mines," *Geofluids*, vol. 2020, pp. 1–15, Article ID 8834347, 2020.

[3] F. Qi, Z. Ma, D. Yang et al., "Stability control mechanism of high-stress roadway surrounding rock by roof fracturing and rock mass filling," *Advances in Civil Engineering*, vol. 2021, Article ID 6658317, pp. 2021–17, 2021.

[4] Q. Wang, B. Jiang, R. Pan et al., "Failure mechanism of surrounding rock with high stress and confined concretesupport system," *International Journal of Rock Mechanics and Mining Sciences*, vol. 102, pp. 89–100, 2018.

[5] S. Mo, K. Tutuk, and S. Saydam, "Management of floor heave at Bulga Underground Operations—a case study," *International Journal of Mining Science and Technology*, vol. 29, no. 1, pp. 73–78, 2019.

[6] H. P. Kang, J. Lin, and M. J. Fan, "Investigation on support pattern of acoal mine roadway within soft rocks—a case study," *International Journal of Coal Geology*, vol. 140, pp. 31–40, 2015.

[7] X. P. Lai, H. C. Xu, P. F. Shan, Y. L. Kang, Z. Y. Wang, and X. Wu, "Research on mechanism and control of floor heave of mining influenced roadway in top coal caving working face," *Energies*, vol. 13, no. 2, p. 381, 2020.

[8] Y. M. Zhao, N. Liu, X. Zheng, and N. Zhang, "Mechanical model for controlling floor heave in deep roadways with U-shaped steel closed support," *International Journal of*

Mining Science and Technology, vol. 25, no. 5, pp. 713–720, 2015.

[9] C. Li, Z. Wang, and T. Liu, "Principle and practice of coupling support of double yielding shell of soft rock roadway under high stress," *International Journal of Mining Science and Technology*, vol. 24, no. 4, pp. 513–518, 2014.

[10] C. Wang, Y. Wang, and S. Lu, "Deformational behaviour of roadways in soft rocks in underground coal mines and principles for stability control," *International Journal of Rock Mechanics and Mining Sciences*, vol. 37, no. 6, pp. 937–946, 2000.

[11] W. Zheng, Y. Zhao, and Q. Bu, "The coupled control of floor heave based on a composite structure consisting of bolts and concrete antiarches," *Mathematical Problems in Engineering*, vol. 2018, Article ID 3545423, pp. 1–14, 2018.

[12] C. Wang, X. Y. Chen, J. D. Zhang, and Y. P. Wu, "Stability mechanism and repair method of U-shaped steel reverse arch support in soft floor roadway," *Advances in Civil Engineering*, vol. 2020, Article ID, 8814365, pp. 1–12, 2020.

[13] A. Chen, X. B. Li, X. S. Liu, Y. L. Tan, K. Xu, and H. L. Wang, ""Relief-Retaining" control technology of floor heave in mining roadway with soft rock: a case study," *Advances in Civil Engineering*, vol. 2021, Article ID 1455052, pp. 1–13, 2021.

[14] T. Yang and J. Zhang, "Research on the treatment technology of soft rock floor heave based on a model of pressure-relief slots," *Arabian Journal of Geosciences*, vol. 14, no. 13, p. 1278, 2021.

[15] Q. Chang, H. Zhou, Z. Xie, and S. Shen, "Anchoring mechanism and application of hydraulic expansion bolts used in soft rock roadway floor heave control," *International Journal of Mining Science and Technology*, vol. 23, no. 3, pp. 323–328, 2013.

[16] M. C. He, G. F. Zhang, G. L. Wang, Y. L. Xu, C. Z. Wu, and Q. D. Tang, "Research on mechanism and application to floor heave control of deep gateway," *Chinese Journal of Mechanical Engineering*, vol. 28, pp. 2593–2598, 2009.

[17] J. Yang, K. Zhou, Y. Cheng, Y. Gao, Q. Wei, and Y. Hu, "Mechanism and control of roadway floor heave in the paleogene soft rock surroundings," *Geotechnical & Geological Engineering*, vol. 37, no. 6, pp. 5167–5185, 2019.

[18] Y. Wang, P. Wang, W. Li, and J. Bai, "Floor heave control technology in deep and soft rock mining roadway: a case study," *Arabian Journal of Geosciences*, vol. 15, no. 6, p. 500, 2022.

[19] Y. Chen, J. Bai, S. Yan, Y. Xu, X. Wang, and S. Ma, "Control mechanism and technique of floor heave with reinforcing solid coal side and floor corner in gob-side coal entry retaining," *International Journal of Mining Science and Technology*, vol. 22, no. 6, pp. 841–845, 2012.

[20] R. Cao, P. Cao, and H. Lin, "Support technology of deep roadway under high stress and its application," *International Journal of Mining Science and Technology*, vol. 26, no. 5, pp. 787–793, 2016.

[21] G. Guo, H. Kang, D. Qian, F. Gao, and Y. Wang, "Mechanism for controlling floor heave of mining roadways using reinforcing roof and sidewalls in underground coal mine," *Sustainability*, vol. 10, no. 5, p. 1413, 2018.

[22] Z. Y. Zhang and H. Shimada, "Numerical study on the effectiveness of grouting reinforcement on the large heaving floor of the deep retained goaf-side gateroad: a case study in China," *Energies*, vol. 11, no. 4, p. 1001, 2018.

[23] H. Shimada, A. Hamanaka, T. Sasaoka, and K. Matsui, "Behaviour of grouting material used for floor reinforcement in underground mines," *International Journal of Mining, Reclamation and Environment*, vol. 28, no. 2, pp. 133–148, 2014.

[24] X. m. Sun, F. Chen, M. c. He, Wl. Gong, Hc. Xu, and H. Lu, "Physical modeling of floor heave for the deep-buried roadway excavated in ten degree inclined strata using infrared thermal imaging technology," *Tunnelling and Underground Space Technology*, vol. 63, pp. 228–243, 2017.

[25] X. M. Zhou, S. Wang, X. L. Li et al., "Research on theory and technology of floor heave control in semicoal rock roadway: taking longhu coal mine in Qitaihe mining area as an Example," *Lithosphere*, vol. 2022, no. 11, Article ID 3810988, 2022.

[26] P. Małkowski, Ł. Ostrowski, and J. Stasica, "Modeling of floor heave in underground roadways in dry and waterlogged conditions," *Energies*, vol. 15, no. 12, p. 4340, 2022.

[27] H. Y. Liu, B. Y. Zhang, X. L. Li et al., "Research on roof damage mechanism and control technology of gob-side entry retaining under close distance gob," *Engineering Failure Analysis*, vol. 138, no. 5, Article ID 106331, 2022.

[28] D. Zhang, J. Bai, Sh. Yan, R. Wang, N. Meng, and G. Wang, "Investigation on the failure mechanism of weak floors in deep and high-stress roadway and the corresponding control technology," *Minerals*, vol. 11, no. 12, p. 1408, 2021.

[29] I. Sakhno, S. Sakhno, and V. Kamenets, "Mechanical model and numerical analysis of a method for local rock reinforcing to control the floor heave of mining-affected roadway in a coal mine," *IOP Conference Series: Earth and Environmental Science*, vol. 970, no. 1, Article ID 012035, 2022.

[30] P. Małkowski, Ł. Ostrowski, and Ł. Bednarek, "The effect of selected factors on floor upheaval in roadways-in situ testing," *Energies*, vol. 13, no. 21, p. 5686, 2020.

[31] I. Sakhno, O. Isayenkov, and S. Rodzin, "Local reinforcing of footing supported in the destroyed rock massif," *Mining of Mineral Deposits*, vol. 11, no. 1, pp. 9–16, 2017.

[32] E. Hoek, C. Carranza-Torres, and B. Corkum, "Hoek-Brown failure criterion – 2002 edition," in *Proceedings of the 5th North American Rock Mechanics Symposium and the 17th Tunnelling Association of Canada Conference, NARMS-TAC, Toronto, Canada*, et al. pp. 267–271, Rocscience Inc, Toronto, Canada, 2002.

[33] M. Cai, P. K. Kaiser, H. Uno, Y. Tasaka, and M. Minami, "Estimation of rock mass deformation modulus and strength of jointed hard rock masses using the GSI system," *International Journal of Rock Mechanics and Mining Sciences*, vol. 41, no. 1, pp. 3–19, 2004.

[34] E. Hoek and M. Diederichs, "Empirical estimation of rock mass modulus," *International Journal of Rock Mechanics and Mining Sciences*, vol. 43, no. 2, pp. 203–215, 2006.

[35] E. T. Brown, *Suggested Methods for Rock Characterization Testing and Monitoring*p. 211, Oxford Pergamon Press, Oxford, UK, 1981.

[36] H. Zhou, C. Zhang, Z. Li, D. Hu, and J. Hou, "Analysis of mechanical behavior of soft rocks and stability control in deep tunnels," *Journal of Rock Mechanics and Geotechnical Engineering*, vol. 6, no. 3, pp. 219–226, 2014.

[37] M. Josh, L. Esteban, C. Delle Piane, J. Sarout, D. N. Dewhurst, and M. B. Clennell, "Laboratory characterisation of shale properties," *Journal of Petroleum Science and Engineering*, vol. 88-89, pp. 107–124, 2012.

[38] I. G. Sakhno, A. V. Molodetskyi, and S. V. Sakhno, "Identification of material parameters for numerical simulation of the behavior of rocks under true triaxial conditions,"

Naukovyi Visnyk Natsionalnoho Hirnychoho Universytetu, vol. 5, pp. 48–53, 2018.

[39] O. A. Almisned and N. B. Alqahtani, "Rock analysis to characterize Saudi soft sandstone rock," *Journal of Petroleum Exploration and Production Technology*, vol. 11, no. 6, pp. 2381–2387, 2021.

[40] Q. Liu, B. Liang, W. Sun, and H. Zhao, "Experimental study on the difference of shale mechanical properties," *Advances in Civil Engineering*, vol. 2021, Article ID 6677992, 14 pages, 2021.